Supplementary Information

Structure of HIV-1 gp120 V1V2 domain with broadly neutralizing antibody PG9

Jason S. McLellan[1#], Marie Pancera[1#], Chris Carrico[2], Jason Gorman[1], Jean-Philippe Julien[3], Reza Khayat[3], Robert Louder[1], Robert Pejchal[3], Mallika Sastry[1], Kaifan Dai[1], Sijy O'Dell[1], Nikita Patel[4], Syed Shahzad-ul-Hussan[1,5], Yongping Yang[1], Baoshan Zhang[1], Tongqing Zhou[1], Jiang Zhu[1], Jeffrey C. Boyington[1], Gwo-Yu Chuang[1], Devan Diwanji[3], Ivelin Georgiev[1], Young Do Kwon[1], Doyung Lee[1], Mark K. Louder[1], Stephanie Moquin[1], Stephen D. Schmidt[1], Zhi-Yong Yang[1], Mattia Bonsignori[6], John A. Crump[7,8], Saidi H. Kapiga[9], Noel E. Sam[8,9], Barton F. Haynes[6], Dennis R. Burton[10, 11], Wayne C. Koff[12], Laura M. Walker[10], Sanjay Phogat[12], Richard Wyatt[10], Jared Orwenyo[13], Lai-Xi Wang[13], James Arthos[4], Carole A. Bewley[5], John R. Mascola[1], Gary J. Nabel[1], William R. Schief[2,10], Andrew B. Ward[3], Ian A. Wilson[3], and Peter D. Kwong[1*]

[1] Vaccine Research Center, National Institute of Allergy and Infectious Diseases, National Institutes of Health, Bethesda, MD 20892, USA.
[2] Department of Biochemistry, University of Washington, Seattle, WA 98195, USA.
[3] Department of Molecular Biology and the Skaggs Institute for Chemical Biology, The Scripps Research Institute, La Jolla, California, USA.
[4] Laboratory of Immunoregulation, National Institutes of Allergy and Infectious Diseases, National Institutes of Health, Bethesda, MD 20892, USA.
[5] Laboratory of Bioorganic Chemistry, National Institute of Diabetes and Digestive and Kidney Diseases, National Institutes of Health, Bethesda, MD 20892, USA.
[6] The Duke Human Vaccine Institute, Duke University School of Medicine, and Duke University Medical Center, Durham, North Carolina 27710, USA.
[7] Division of Infectious Diseases and International Health, Department of Medicine, and Department of Pathology, Duke University Medical Center, Durham, North Carolina 27710, USA.
[8] Kilimanjaro Christian Medical Centre and Kilimanjaro Christian Medical College, Tumaini University, Moshi, Tanzania.
[9] Kilimanjaro Reproductive Health Programme, Moshi, Tanzania.
[10] Department of Immunology and Microbial Science and IAVI Neutralizing Antibody Center, The Scripps Research Institute, La Jolla, California 92037, USA.
[11] Ragon Institute of MGH, MIT, and Harvard, Cambridge, Massachusetts 02129, USA.
[12] International AIDS Vaccine Initiative (IAVI), New York, NY 10038, USA.
[13] Institute of Human Virology and Department of Biochemistry & Molecular Biology, University of Maryland School of Medicine, Baltimore, Maryland 21201, USA.

[#]Equal contribution

[*]Correspondence should be addressed to P.D.K. Vaccine Research Center, NIAID/NIH
40 Convent Drive; Building 40, Room 4508, Bethesda, MD 20892; Phone: (301) 594-8685; Fax: (301) 480-2658, E-mail: pdkwong@nih.gov.

Table of contents

Supplementary Table 1. Variational crystallization of gp120s containing the V1V2 region

Complex #	gp120	Ligands						# Ligands	Hits
		D1D2	17b	48d	M48U1	NBD557	BMS806		
1	YU2 44-492 ΔV3							0	0
2	YU2 44-492 ΔV3	X		X				2	0
3	YU2 44-492 ΔV3	X	X		X			3	0
4	YU2 44-492 ΔV3	X		X	X			3	0
5	YU2 83-491 ΔV3 new	X		X				2	0
6	YU2 83-491 ΔV3 new	X	X					2	0
7	YU2							0	0
8	C1086 44-492 ΔV3	X						0	0
9	ZM53 44-492	X	X					2	0
10	ZM53 44-492							0	0
11	ZM53 44-492					X		1	0
12	ZM53 44-492						X	1	**1**
13	ZM53 44-492 glyc							0	0
14	ZM109 44-492							0	0
15	ZM109						X	1	0
16	ZM109							0	0
17	ZM197 44-492						X	1	0
18	CAP45 44-492						X	1	0
19	ZM248M 44-492							0	0
20	ZM249M 44-492 glyc							0	0
21	DU123.06							0	0
22	DU172.17							0	0
23	CAP244							0	0
24	HXBc2 83-491 ΔV3 new	X	X					2	0
25	SF162 44-492 ΔV3	X		X				2	0
26	SF162 44-492 ΔV3 new							0	0

Mammalian codon-optimized genes encoding full length, 44-492 (HXBc2 numbering), or V3 loop-deleted gp120s from various strains were synthesized with a human CD5 leader (ΔV3: V3 residues have been replaced as follows: 297-GAG-330, ΔV3 new: V3 residues have been replaced as follows: 302-GGSGSGG-325).The genes were cloned into the XbaI/BamHI sites of the mammalian expression vector pVRC8400, and transiently transfected into HEK293S GnTI$^{-/-}$ cells. gp120 proteins were purified from the media using a 17b affinity column, eluted with IgG elution buffer (Pierce) and immediately neutralized by adding 1M Tris-HCl pH 8.5. The proteins were flash frozen in liquid nitrogen and stored at -80 ºC until further use. Complexes or unbound gp120 (with and without *N*-linked glycans) were used for crystallization screening. All proteins were passed over a 16/60 S200 size exclusion column. Monodisperse fractions were pooled, and after concentration, proteins were screened against 576 crystallization conditions using a Cartesian Honeybee crystallization robot. Initial crystals were grown by the vapor diffusion method in sitting drops at 20ºC by mixing 0.2 µl of protein complex with 0.2 µl of reservoir solution.

Supplementary Table 2. Expression of large V1V2 scaffolds

Scaffold PDB ID*	Chain ID	Expression (mg/L)
1DQG	A	1.0
3HEI	A	<0.1
3AL9	A	<0.1
3FBX	A	<0.1
2BCE	A	<0.1
3HRZ	D	<0.1

*Scaffolds described in Supplementary Table 3.

Supplementary Table 3. V1V2 scaffolds

PDB	Protein	Length[i]	Insertion[ii]	Mutations/Insertions	Sequence As Computationally Designed[iii]
1CHL	*L quinquestriatus* chlorotoxin	36	30-31	Y29A	MCMPCFTTDHQMARKCDDCCGGKGRGKCA**CVG AGSC**CTCLCR
2BRZ	*P brazzeana* sweet protein	54	39-45	None	DKCKKVYENYPVSKCQLANQCNYDCKLDKHAR SGECF**CVGAGSC**QCICDYCEY
1IW4	*H roretzi* trypsin inhibitor	55	25-30	E31Q, E32T	AHMDCTEFNPLCRCNKMLGDLICA**CVGAGSC**QT HRNMCALCCEHPGGFEYSNGPCE
1FD6	Designed Protein G B1 domain	57	9-15	I7A, I8A, G15Q, E16T	MTTFKLAA**CVGAGSC**QTTTTEAVDAATAEKVFK QYANDNGIDGEWTYDDATKTFTVTE
1JO8	Stabilized *S cerevisiae* Abp1 SH3 domain	58	42-43	None	GPWATALYDYDAAEDNELTFKEGDKIINIEFVDD DWWLGELE**CVGAGSC**GSKGLFPSNYVSLGN
1E6G	Chicken spectrin SH3 domain	62	46-49	I25V	TGKELVLVLYDYQEKSPRELTVKKGDILTLLNST NKDWWKVE**CVGAGSC**QGFIPAAYLKKLD
1G6M	*Naja kaouthia* CBT 2	62	32-33	D31L, G34N	LECHNQQSSQTPTTTGCSGGENNCYKKEWRL**CV GAGSC**NYRTERGCGCPSVKKGIGINCCTTDRCNN
1QPM	Mu phage repressor domain	69	38-44	K37L, A45V	KSIWCSPQEIMAADGMPGSVAGVHYRANVQGWT KRKF**CVGAGSC**TVEYDVMSMPTKEREQVIAHLG LST
1XQQ	*H sapiens* ubiquitin	76	46-47	F45L, K48Q	MQIFVKTLTGKTITLEVEPSDTIENVKAKIQDKEGI PPDQQRLIA**CVGAGSC**QQLEDGRTLSDYNIQKES TLHLVLRLRGG
1IP9	*S cerevisiae* PB1 domain	85	20-21	Y19L, D22N, D84P	GAMGSSTSGLKTTKIKFYL**CVGAGSC**NIFALMLK GDTTYKELRSKIAPRIDTDNFKLQTKLFDGSGEEI KTDSQVSNIIQAKLKISVHPI
1XBD	*C fimi* xylan binding domain	87	53-59	G51P, S52L, T60N	TGCSVTATRAEEWSDRFNVTYSVSGSSAWTVNL ALNGSQTIQASWNANVTTD**CVGAGSC**TRTVTPN GSGNTFGVTVMKNGSSTTPAATCAGS
1DQG	*M musculus* mannose receptor cysteine-rich domain	135	19-23	VGS inserted pre-V1V2, YFF inserted post-V1V2	LDARQFLIYNEDHKRCVDAVGS**CVGAGSC**YFFV QTATCNPEAESQKFRWVSDSQIMSVAFKLCLGVP SKTDWASVTLYACDSKSEYQKWECKNDTLFGIK GTELYFNYGNRQEKNIKLYKGSGLWSRWKVYGT TDDLCSRGYE
3HEI	*H sapiens* ephrin receptor 2 fragment	160	30-37	VLV inserted pre-V1V2, LFV inserted post-V1V2	EVVLLDFAAAGGELGWLTHPYGKGWDLMQVLV **CVGAGSC**LFVYMYSVCNVMSGDQDNWLRTNW VYRGEAERIFIELKFTVRDCNSFPGGASSCKETFN LYYAESDLDYGTNFQKRLFTKIDTIAPDEITVSSDF EARHVKLNVEERSVGPLTRKGFYLAFQDIGACVA LLSVRVYYKKC
3AL9	*M musculus* plexin A2	539	255-258	WYED inserted pre-V1V2, DRVF inserted post-V1V2	GTTGMPQYSTFHSENRDWTFNHLTVHRRTGAVY VGAINRVYKLTGNLTIQVAHKTGPEEDNKACYPP LIVQPCSEVLTLTNNVNKLLIIDYSENRLLACGSLY QGVCKLLRLDDLFILVEPSHKKEHYLSSVNKTGT MYGVIVRSEGEDGKLFIGTAVDGKQDYFPTLSSR KLPRDPESSAMLDYELHSDFVSSLIKIPSDTLALVS HFDIFYIYGFASGGFVYFLTVQPETPDGMAINSAG DLFYTSRIVRLCKDDPKFHSYVSLPFGCWYED**CV GAGSC**DRVFYRLLQAAYLAKPGEALAQAFNISSD EDVLFAIFSKGQKQYHHPPDDSALCAFPIRAINLQI KERLQSCYHGEGNLELNWLLGKDVQCTKAPVPI DDNFCGLDINQPLGGSTPVEGLTLYTTSRDRLTSV ASYVYNGYSVVFVGTKSGKLKKIRADGPPHGGV QYEMVSVFKDGSPILRDMAFSINQLYLYVMSERQ VTRVPVESCEQYTTCGECLSSGDPHCGWCALHN MCSRRDKCQRAWEANRFAASISQCMSSRENLYF Q

3FBX	*M musculus* lysosomal protein	559	183-188	YAW inserted pre-V1V2, LGM inserted post-V1V2	LPTLGPGWQRQNPDPPVSRTRSLLLDAASGQLRL EDGFHPDAVAWANLTNAIRETGWAYLDLSTNGR YNDSLQAYAAGVVEASVSEELIYMHWMNTVVN YCGPFEYEVGYCEKLKNFLEANLEWMQREMELN PDSPYWHQVRLTLLQLKGLEDSYEGRLTFPTGRF TIKPLGFLLLQISGDLEDLEPALNKTNTKPSLGSGS SALIKLYAW**CVGAGSC**LGMLLVAHNTWNSYQN MLRIIKKYRLQFREGPQEEYPLVAGNNLVFSSYPG TIFSGDDFYILGSGLVTLETTIGNKNPALWKYVQP QGCVLEWIRNVVANRLALDGATWADVFKRFNSG TYNNQWMIVDYKAFLPGGPSPGSRVLTILEQIPG MVVVADKTAELYKTTYWASYNIPYFETVFNASG LQALVAQYGDWFSYTKNPRAKIFQRDQSLVEDM DAMVRLMRYNDFLHDPLSLCEACNPKPNAENAIS ARSDLNPANGSYPFQALHQRAHGGIDVKVTSFTL AKYMSMLAASGPTWDQCPPFQWSKSPFHSMLH MGQPDLWMFSPIRVPWDGRGS
2BCE	*B taurus* cholesterol esterase	579	19-26	DGT inserted pre-V1V2 LVP inserted post-V1V2	AKLGSVYTEGGFVEGVNKDGT**CVGAGSC**LVPVD IFKGIPFAAAPKALEKPERHPGWQGTLKAKSFKK RCLQATLTQDSTYGNEDCLYLNIWVPQGRKEVSH DLPVMIWIYGGAFLMGASQGANFLSNYLYDGEEI ATRGNVIVVTFNYRVGPLGFLSTGDSNLPGNYGL WDQHMAIAWVKRNIEAFGGDPDQITLFGESAGG ASVSLQTLSPYNKGLIKRAISQSGVGLCPWAIQQD PLFWAKRIAEKVGCPVDDTSKMAGCLKITDPRAL TLAYKLPLGSTEYPKLHYLSFVPVIDGDFIPDDPV NLYANAADVDYIAGTNDMDGHLFVGMDVPAINS NKQDVTEEDFYKLVSGLTVTKGLRGAQATYEVY TEPWAQDSSQETRKKTMVDLETDILFLIPTKIAVA QHKSHAKSANTYTYLFSQPSRMPIYPKWMGADH ADDLQYVFGKPFATPLGYRAQDRTVSKAMIAYW TNFARTGDPNTGHSTVPANWDPYTLEDDNYLEIN KQMDSNSMKLHLRTNYLQFWTQTYQALPTVTSA GASLLPPEDNSQASPVPPADNSGAPTEPSAGDSEV AQMPVVIGF
3HRZ	*H sapiens* complement factor B	741	444-449	KWAL inserted pre-V1V2, QFFM inserted post-V1V2	TPWSLARPQGSCSLEGVEIKGGSFRLLQEGQALEY VCPSGFYPYPVQTRTCRSTGSWSTLKTQDQKTVR KAECRAIHCPRPHDFENGEYWPRSPYYNVSDEISF HCYDGYTLRGSANRTCQVNGRWSGQTAICDNGA GYCSNPGIPIGTRKVGSQYRLEDSVTYHCSRGLTL RGSQRRTCQEGGSWSGTEPSCQDSFMYDTPQEVA EAFLSSLTETIEGVDAEDGHGPGEQQKRKIVLDPS GSMNIYLVLDGSGSIGASDFTGAKKCLVNLIEKV ASYGVKPRYGLVTYATYPKIWVKVSEADSSNAD WVTKQLNEINYEDHKLKSGTNTKKALQAVYSM MSWPDDVPPEGWNRTRHVIILMTDGLHNMGGDP ITVIDEIRDLLYIGKDRKNPREDYLDVYVFGVGPL VNQVNINALASKKDNEQHVFKVKDMENLEDVFY QMIDESQSLSLCGMVWEHRKGTDYHKQPWQAKI KWAL**CVGAGSC**QFFMCMGAVVSEYFVLTAAHC FTVDDKEHSIKVSVGGEKRDLEIEVVLFHPNYNIN GKKEAGIPEFYDYDVALIKLKNKLKYGQTIRPICL PCTEGTTRALRLPPTTTCQQQKEELLPAQDIKALF VSEEEKKLTRKEVYIKNGDKKGSCERDAQYAPG YDKVKDISEVVTPRFLCTGGVSPYADPNTCRGDS GGPLIVHKRSRFIQVGVISWGVVDVCKNQKRQKQ VPAHARDFHINLFQVLPWLKEKLQDEDLGFLAA

[i]Number of residues before deletion of native segment and insertion of V1V2 stub.

[ii]Residue range listed was removed from the native structure for the V1V2 insertion procedure.

[iii]CVGAGSC is a placeholder sequence for the V1V2 stub used in our modeling software, derived from PDB ID 1RZJ. Any V1V2 sequence can likely be inserted in place of the stub.

Supplementary Table 4. Peptide mapping of V1V2-directed murine monoclonal antibodies

Protein or peptide	SBS01	SBS02	SBS03	SBS04	SBS05	SBS06	F105	9E8
YU2gp120FL	++	++	++	++	++	++	++	-
YU2gp120 ΔV1V2	-	-	-	-	-	-	++	-
V1 (T_{133}-E_{147})	-	-	-	-	-	-	-	-
V1 (S_{143}-C_{157})	-	+	-	-	++	-	-	-
V1V2 (E_{153}-D_{167})	-	-	-	-	-	-	-	-
V2 (T_{163}-Y_{177})	+	-	+/-	+	-	-	-	-
V2 (Y_{173}-A_{187})	-	-	-	-	-	-	-	-
V2 (P_{183}-S_{197})	-	-	-	-	-	+/-	-	-
V2 (S_{193}-S_{207})	-	-	-	-	-	-	-	-

Monoclonal antibodies against the V1V2 domain were obtained from ProSci. These antibodies were generated by immunizing mice with YU2 gp120 and the sera were tested against YU2 gp120 ΔV1V2 to select positive wells. Six YU2-V1V2 specific monoclonal antibodies (SBS01-06, subtype IgG1, IgG2a) were obtained. Peptide mapping was performed by ELISA. Serial dilutions of the six V1V2-directed antibodies were added to YU2 V1V2 peptide-coated wells and binding was probed with horseradish peroxidase-conjugated anti-mouse IgG antibody. YU2 gp120 and gp120 ΔV1V2 were used as positive and negative controls, respectively. Anti-HIV-1 antibody F105 and anti influenza hemagglutinin antibody 9E8 were also used as control antibodies.

Supplementary Table 5. Antibody and integrin recognition of YU2 V1V2 scaffolds

	SBS01	SBS02	SBS03	SBS04	SBS05	SBS06	$\alpha_4\beta_7$
YU2gp120 FL	++	++	++	++	++	++	+
YU2gp120 ΔV1V2	-	-	-	-	-	-	-
1FD6 V1V2*#	++	++	++	++	++	++	+
1XQQ V1V2	+/-	+/-	+/-	+/-	+/-	-	-
1XBD V1V2	-	-	-	-	-	-	ND
2BRZ V1V2	-	-	-	-	-	-	ND
1IW4 V1V2	-	-	-	+/-	-	-	ND
1G6M V1V2	-	-	-	-	+/-	-	ND
1QPM V1V2	+/-	-	+/-	+/-	+/-	-	-
1JO8 V1V2#	+/-	+/-	+/-	+/-	+/-	+/-	+
1E6G V1V2#	+/-	+/-	+/-	+/-	+/-	+/-	-
1IP9 V1V2	-	-	-	-	-	-	ND
1CHL V1V2	-	-	-	-	-		ND

*1FD6 scaffold protein is a variant of the B1 domain of streptococcal protein G, which binds the Fc region of antibodies and could contribute to binding in the ELISA assay, however this scaffold also binds $\alpha_4\beta_7$ in the competition assay.
#These scaffold proteins were tested with surface plasmon resonance and biolayer interferometry.

Antigenic analysis of the YU2 V1V2 scaffolds was initially performed by sandwich ELISA. YU2 V1V2 scaffolds were expressed as GFP fusion proteins. The expressed V1V2 scaffold proteins in culture supernatants were added in duplicate to wells coated with a goat polyclonal anti-GFP antibody (Santa Cruz) to allow capture of the desired protein. SBS01-06 proteins were used as detection antibodies and binding was probed with horseradish peroxidase-conjugated anti-mouse IgG antibody. Full length YU2 gp120, ΔV1V2, and secreted GFP were used as control proteins and antibodies. A subset of purified V1V2 scaffold proteins was antigenically characterized by surface plasmon resonance and biolayer interferometry.

Supplementary Table 6. ELISA binding of PG9 and PG16 to clade B and C gp120 monomers

Clade B					Clade C and negative controls				
gp120	PG9	PG16	VRC01	HIV-IG	gp120	PG9	PG16	VRC01	HIV-IG
6535.3	+++	+++	++++	+++	CAP45.2.00.G3	++++	+++	+++	+++
AC10.0.29	++	-	+++	+++	CAP210.2.00.E8	+	-	++	+++
BaL.01	++++	-	++++	+++	CAP244.2.00.D3	-	-	+++	+++
CAAN5342.A2	+++	+	++++	+++	Du151.2	+	-	++++	+++
HXB2	++	-	++++	+++	Du156.12	++	-	++++	+++
PVO.4	+	-	+++	+++	Du172.17	+++	-	+	+++
QH0692.42	-	-	++++	+++	Du422.1	++	-	-	+++
R2	-	-	+++	+++	ZM53M.PB12	++++	+++	++++	+++
REJO4541.67	+++	+	++++	+++	ZM109F.PB4	++++	+++	++++	+++
RHPA4259.7	++	-	++++	+++	ZM135M.PL10a	-	-	+++	+++
SC422661.8	++++	+	++++	+++	ZM197M.PB7	++++	++	++++	+++
TRJO4551.58	+++	++	+++	+++	ZM214M.PL15	+	-	++++	+++
THRO4156.18	+++	+	++++	+++	ZM233M.PB6	+++	+++	++	+++
TRO.11	++	-	+++	+++	ZM249M.PL1	+++	+	++++	+++
WITO4160.33	++	-	+++	+++	SIVmac239 gp140	-	-	-	++
YU2	++	-	++++	+++	SIVmac251.30 gp140	-	-	+	+++
					H5 HA1	-	-	-	+

Purified recombinant gp120 (200 ng) was adsorbed onto Reacti-Bind 96-well plates (Pierce), followed by blocking and incubation of serially diluted antibodies. Bound antibody was detected using a horseradish peroxidase-conjugated goat anti-human IgG Fc antibody (Jackson ImmunoResearch Laboratories). Plates were developed using SureBlue 3,3',5,5'-tetramethylbenzidine (Kirkegaard & Perry Laboratories). gp120 proteins were purchased from Immune Technology Corp. or were expressed and purified as described in Supplementary Table 1. Binding was categorized based on the OD_{450} value at the highest concentration tested (5 mg/ml for mAbs, 50 mg/ml for HIV-IG) and EC_{50} values as follows: '++++' = $OD_{450} \geq 3.0$ and $EC_{50} \leq 0.10$; '+++' = $OD_{450} \geq 3.0$ and $EC_{50} > 0.10$; '++' = $1.0 \leq OD_{450} < 3.0$; '+' = $0.2 \leq OD_{450} < 1.0$; '-' = $OD_{450} < 0.2$. OD values were rounded to the nearest tenth and EC_{50} values to the nearest hundredth before categorization. mAb VRC01 and HIV-IG were included as control antibodies and SIV gp140 proteins and avian influenza hemagglutinin HA1 (H5 HA1) were included as control proteins.

Supplementary Table 7. Data collection and refinement statistics for V1V2 scaffolds complexed with PG9 Fab

	1FD6-CAP45/PG9	1FD6-ZM109/PG9
Data collection		
Space group	$P2_12_12_1$	$P2_1$
Cell dimensions		
a, *b*, *c* (Å)	73.0, 103.5, 186.4	89.5, 86.6, 94.9
α, β, γ (°)	90.0, 90.0, 90.0	90.0, 92.1, 90.0
Resolution (Å)	50.0-2.2 (2.24-2.19)*	50.0-1.8 (1.83-1.80)*
R_{sym} or R_{merge}	11.2 (33.9)	6.3 (43.8)
$I / \sigma I$	8.7 (2.4)	20.3 (2.0)
Completeness (%)	92.0 (68.7)	91.2 (64.8)
Redundancy	4.1 (2.4)	3.7 (2.9)
Molecules/ASU	2	2
Refinement		
Resolution (Å)	30.0-2.19	41.6-1.80
No. reflections	67,671	122,322
R_{work} / R_{free}	0.182/0.234	0.178/0.205
No. atoms	10,341	10,152
Protein	9,507	9,074
Ligand/ion	348	231
Water	487	847
B-factors		
Protein	46.0	45.7
Ligand/ion	71.9	43.3
Water	43.4	42.1
R.m.s. deviations		
Bond lengths (Å)	0.009	0.007
Bond angles (°)	1.09	1.07
PDB ID	3U4E	3U2S

*Values in parentheses are for highest-resolution shell. Each data set was collected from a single crystal.

Supplementary Table 8. Structural characterization of HIV-1 gp120

Structure	Residues in structure (HXB2 numbering)*	Residues in mature gp120 that remained to be defined crystallographically	Crystallization ligand(s)	Reference
HIV-1 gp120 core ΔC1C5ΔV1V2ΔV3 strain HXBc2	83-127, 195-297, 330-492	31-82, 128-194, 298-329, 493-511	CD4 (d1d2), 17b	Kwong et al., Nature, 1998
HIV-1 gp120 core + V3 ΔC1C5ΔV1V2 strain JR-FL	83-127, 195-492	31-82, 128-194, 493-511	CD4 (d1d2), X5	Huang et al., Science, 2005
HIV-1 gp120 core + N/C ΔV1V2ΔV3 strain HXBc2	31-123, 199-297, 330-511	128-194	CD4 (d1d2), 48d	Pancera et al., PNAS, 2010
HIV-1 gp120 V1V2 strains ZM109 and CAP45	126-196	none	PG9	Current

*The mature protein is comprised of residues 31-511.

Supplementary Table 9. Interactions between CAP45 V1V2 scaffold and PG9 Fab

A. CAP45-Protein : PG9-Protein interactions

	Interface Residue	Bond Type	ASA	BSA	Δ_iG
CAP45	CAP45:SER 158		31.11	3.86 ||	0.06
	CAP45:ASN 160		88.58	39.38 |||||	-0.23
	CAP45:THR 162		65.55	6.14 |	0.03
	CAP45:THR 163		64.39	0.37 |	-0.00
	CAP45:GLU 164		82.79	0.24 |	-0.00
	CAP45:LEU 165		139.58	4.53 |	0.07
	CAP45:ARG 166	H	225.48	40.18 ||	0.01
	CAP45:ASP 167	H	106.95	34.99 ||||	-0.29
	CAP45:LYS 168	HS	117.90	78.82 ||||||	-0.22
	CAP45:LYS 169	H	130.55	102.54 |||||||	0.72
	CAP45:GLN 170	H	103.11	69.70 ||||||	-0.05
	CAP45:LYS 171	H	153.85	90.29 ||||||	0.52
	CAP45:ALA 172		25.17	7.26 |||	0.12
	CAP45:TYR 173		147.52	17.94 ||	0.29
PG9	H:ARG 31		47.00	0.29 |	-0.01
	H:ARG 100B		103.55	9.77 |	-0.14
	H:GLY 100D		57.64	14.72 |||	-0.17
	H:TYR 100E	H	148.93	113.74 |||||||	0.87
	H:ASN 100F	H	82.37	30.92 ||||	-0.22
	H:TYS 100G		122.49	69.66 ||||||	0.59
	H:TYS 100H	H	121.32	59.02 |||||	-0.20
	H:ASP 100I	H	24.40	14.01 |||||	-0.07
	H:PHE 100J		155.15	97.54 ||||||	1.52
	H:TYR 100K		194.18	20.13 ||	0.08
	H:ASP 100L	HS	74.70	47.17 ||||||	-0.24
	H:TYR 100O		89.21	19.92 |||	-0.17

Bond type: H: **H**ydrogen, S: **S**alt bridge
ASA Accessible Surface Area, Å^2
BSA BuriedSurfaceArea,Å^2
Δ_iG Solvation energy effect, kcal/mol
||||Buried area percentage, one bar per 10%
Detailed interface data was calculated on the EBI PISA server (http://www.ebi.ac.uk/msd-srv/prot_int/cgi-bin/piserver)

B. CAP45-Glycan : PG9-Protein interactions

Interface Residue	Bond Type	ASA	BSA	Δ_iG
CAP45:NAG 656-PG9:H		361.41	36.62 ||	-1.05
H:GLU 56		77.43	2.00 |	-0.03
H:PHE 100J		155.15	31.56 |||	0.51
CAP45:NAG 657-PG9:H	H	362.60	122.88 ||||	-2.52
H:ASP 53		53.25	5.50 ||	-0.09
H:SER 55		76.26	37.26 |||||	0.44
H:PHE 100J		155.15	24.25 ||	0.39
H:TYR 100K	H	194.18	35.17 ||	0.17
CAP45:MAN 658-PG9:H		289.03	48.25 ||	-0.81
H:ASP 53		53.25	0.61 |	-0.01
H:GLY 54		24.47	9.22 ||||	-0.06
H:SER 55		76.26	27.76 ||||	0.30
CAP45:MAN 659-PG9:H	H	288.45	86.97 ||||	-0.91
H:GLY 54	H	24.47	9.57 ||||	-0.11
H:SER 55	H	76.26	11.24 ||	-0.04
H:GLU 56		77.43	2.18 |	0.03
H:LYS 57	H	94.60	40.92 |||||	-0.34
H:SER 70		40.32	0.50 |	0.01
CAP45:MAN 660-PG9:H		288.61	10.75 |	-0.25
H:TYR 100K		194.18	11.03 |	-0.00
CAP45:MAN 662-PG9:H	H	291.08	123.55 |||||	-1.79
H:SER 30		49.55	2.34 |	0.04
H:ASP 53		53.25	24.81 |||||	0.10
H:ASN 73	H	47.36	20.56 |||||	0.03
H:TYR 100K		194.18	40.78 |||	0.55

Bond type: H: **H**ydrogen, S: **S**alt bridge
ASA Accessible Surface Area, $Å^2$
BSA BuriedSurfaceArea,$Å^2$
Δ_iG Solvation energy effect, kcal/mol
|||| Buried area percentage, one bar per 10%
Detailed interface data was calculated on the EBI PISA server (http://www.ebi.ac.uk/msd-srv/prot_int/cgi-bin/piserver)

B. (cont'd) CAP45-Glycan : PG9-Protein interactions

Interface Residue	Bond Type	ASA	BSA	$\Delta_i G$
CAP45:NAG 560-PG9:H	H	362.10	123.39 ||||	-2.04
H:ASP 100	H	64.98	8.99 ||	-0.07
H:ARG 100B	H	103.55	32.01 ||||	-0.35
H:TYS 100G		122.49	23.42 ||	0.18
H:TYR 100O		89.21	19.12 |||	-0.05
CAP45:NAG 561-PG9:H	H	362.52	91.85 |||	-2.63
H:ASP 100	H	64.98	25.49 ||||	-0.01
H:ARG 100B		103.55	12.87 ||	-0.22
H:TYR 100O		89.21	26.17 |||	0.41
CAP45:MAN 562-PG9:L		286.50	8.13 |	-0.24
L:TYR 30		75.49	7.86 ||	0.13
CAP45:MAN 564-PG9:H		286.69	32.35 ||	-0.40
H:ASP 100		64.98	2.91 |	0.00
H:ASN 100P		52.24	0.98 |	-0.01
H:HIS 100R		153.38	28.66 ||	0.20
CAP45:MAN 564-PG9:L		286.69	54.34 ||	-0.73
L:TYR 30		75.49	22.70 ||||	0.36
L:GLU 31		111.38	10.91 |	0.13
L:SER 32		39.82	7.04 ||	-0.08
L:LEU 91		43.42	8.46 ||	0.14
CAP45:MAN 565-PG9:H	H	284.85	76.50 |||	-0.32
H:ASP 100		64.98	6.20 |	-0.11
H:ASN 100P		52.24	2.58 |	-0.03
H:TYR 100Q		100.63	22.87 |||	0.16
H:HIS 100R	H	153.38	20.14 ||	-0.00
CAP45:MAN 565-PG9:L	H	284.85	110.93 ||||	-2.08
L:GLU 31		111.38	22.00 ||	0.29
L:SER 32	H	39.82	12.65 ||||	-0.13
L:ASP 50		54.82	31.73 |||||	-0.15
L:LYS 53	H	100.49	14.07 ||	-0.50
CAP45:MAN 566-PG9:H	H	289.57	97.00 ||||	-1.09
H:TYR 100O		89.21	24.01 |||	0.38
H:ASN 100P	H	52.24	23.54 |||||	-0.24
H:HIS 100R	H	153.38	26.35 ||	0.49
CAP45:MAN 566-PG9:L		289.57	91.51 ||||	-1.19
L:TYR 30		75.49	9.88 ||	0.08
L:LEU 91		43.42	17.50 |||||	0.28
L:THR 92		1.09	0.49 |||||	-0.01
L:ARG 95		202.42	44.97 |||	-0.58
L:ARG 96		149.20	10.25 |	-0.35

Bond type: H: **H**ydrogen, S: **S**alt bridge
ASA Accessible Surface Area, $Å^2$
BSA BuriedSurfaceArea,$Å^2$
$\Delta_i G$ Solvation energy effect, kcal/mol
|||| Buried area percentage, one bar per 10%
Detailed interface data was calculated on the EBI PISA server (http://www.ebi.ac.uk/msd-srv/prot_int/cgi-bin/piserver)

Supplementary Table 10. Interactions between ZM109 V1V2 scaffold and PG9 Fab

A. ZM109-Protein : PG9-Protein interactions

	Interface Residue	Bond Type	ASA	BSA	Δ_iG
	ZM109:CYS 157		8.96	1.72 ||	-0.02
	ZM109:SER 158		27.85	6.02 |||	0.10
	ZM109:ASN 160		80.18	35.40 |||||	-0.17
	ZM109:THR 162		14.08	2.33 ||	-0.03
	ZM109:LYS 166		140.78	11.39 |	-0.13
ZM109	ZM109:ASP 167	H	133.11	55.17 |||||	0.14
	ZM109:ARG 168	HS	150.27	99.54 |||||||	-0.92
	ZM109:LYS 169	H	92.29	91.51 |||||||||	0.19
	ZM109:GLN 170		113.66	65.25 ||||||	-0.09
	ZM109:LYS 171	HS	141.53	91.21 |||||||	-0.09
	ZM109:VAL 172		45.81	0.31 |	0.01
	ZM109:ASN 173	H	135.28	60.34 |||||	0.20
	H:ARG 31		42.07	1.01 |	-0.04
	H:ARG 100B		99.05	8.00 |	-0.30
	H:GLY 100D		58.60	14.18 |||	-0.16
	H:TYR 100E	H	138.43	98.50 |||||||	0.85
	H:ASN 100F	H	90.98	41.07 |||||	-0.28
PG9	H:TYS 100G	H	126.29	85.17 ||||||	0.38
	H:TYS 100H	H	125.91	68.59 ||||||	0.06
	H:ASP 100I	HS	32.23	21.66 ||||||	-0.21
	H:PHE 100J		145.90	97.54 ||||||	1.54
	H:TYR 100K	H	179.08	46.70 |||	-0.06
	H:ASP 100L	HS	73.70	35.34 |||||	-0.08
	H:TYR 100O		83.78	20.22 |||	-0.13

Bond type: H: **H**ydrogen, S: **S**alt bridge
ASA Accessible Surface Area, $Å^2$
BSA BuriedSurfaceArea,$Å^2$
Δ_iG Solvation energy effect, kcal/mol
||||Buried area percentage, one bar per 10%
Detailed interface data was calculated on the EBI PISA server (http://www.ebi.ac.uk/msd-srv/prot_int/cgi-bin/piserver)

B. ZM109-Glycan : PG9-Protein interactions

Interface Residue	Bond Type	ASA	BSA	$\Delta_i G$
ZM109:NAG 560-PG9:H	H	360.05	126.97 ||||	-2.32
H:ASP 100	H	59.01	10.14 ||	-0.08
H:ARG 100B	H	99.05	26.55 |||	-0.36
H:TYS 100G		126.29	23.20 ||	0.21
H:TYR 100O		83.78	19.41 |||	-0.03
ZM109:NAG 561-PG9:H		361.72	86.56 |||	-2.49
H:ASP 100		59.01	24.98 |||||	-0.00
H:ARG 100B		99.05	11.69 ||	-0.26
H:TYR 100O		83.78	22.80 |||	0.36
ZM109:MAN 562-PG9:L		290.21	7.54 |	-0.25
L:TYR 30		72.56	7.14 |	0.11
ZM109:MAN 564-PG9:H		288.35	32.43 ||	-0.41
H:ASP 100		59.01	1.30 |	-0.02
H:ASN 100P		57.91	1.22 |	-0.01
H:HIS 100R		153.20	30.19 ||	0.71
ZM109:MAN 564-PG9:L		288.35	49.24 ||	-0.65
L:TYR 30		72.56	19.58 |||	0.31
L:GLU 31		109.49	6.31 |	0.06
L:SER 32		38.09	5.51 ||	-0.06
L:LEU 91		44.38	9.41 |||	0.15
ZM109:MAN 565-PG9:H	H	291.61	78.19 |||	-0.20
H:ASP 100		59.01	8.70 ||	-0.15
H:ASN 100P		57.91	2.82 |	-0.03
H:TYR 100Q		95.03	19.22 |||	0.10
H:HIS 100R	H	153.20	21.99 ||	0.01
ZM109:MAN 565-PG9:L	H	291.61	108.26 ||||	-2.20
L:TYR 30		72.56	0.16 |	0.00
L:GLU 31		109.49	19.78 ||	0.17
L:SER 32	H	38.09	12.62 ||||	-0.09
L:ASP 50		49.15	28.76 |||||	-0.19
L:LYS 53		104.44	12.48 ||	-0.44
ZM109:MAN 566-PG9:H	H	292.40	100.98 ||||	-1.12
H:TYR 100O		83.78	21.34 |||	0.34
H:ASN 100P	H	57.91	25.01 |||||	-0.26
H:HIS 100R	H	153.20	26.23 ||	0.51
ZM109:MAN 566-PG9:L		292.40	87.27 |||	-1.17
L:TYR 30		72.56	7.27 ||	0.10
L:LEU 91		44.38	17.63 ||||	0.28
L:ARG 95		205.09	44.09 |||	-0.42
L:ARG 96		148.86	10.56 |	-0.37
ZM109:NAG 573-PG9:H	H	361.83	101.33 |||	-2.89
H:LYS 52		50.77	1.71 |	-0.06
H:ASP 53		53.71	5.03 |	-0.09
H:SER 55		71.82	19.19 |||	0.24
H:PHE 100J		145.90	28.94 ||	0.46
H:TYR 100K	H	179.08	32.94 ||	-0.15

Bond type: H: **H**ydrogen, S: **S**alt bridge
ASA Accessible Surface Area, $Å^2$
BSA BuriedSurfaceArea,$Å^2$
$\Delta_i G$ Solvation energy effect, kcal/mol
|||| Buried area percentage, one bar per 10%
Detailed interface data was calculated on the EBI PISA server (http://www.ebi.ac.uk/msd-srv/prot_int/cgi-bin/piserver)

Supplementary Table 11. EC_{50} (µg/mL) of PG9 and PG16 binding to V1V2 scaffolds and to associated glycosylation mutants

1FD6 ZM109 scaffold	WT	N130D	N138D	N160Q	N173D	N189D	N192D
PG9	0.1	0.4	0.2	-	7.0	0.1	0.1
PG16	3.4	1.5	4.4	-	-	4.0	2.5

"-" indicates no binding or EC_{50}>50µg/mL

1FD6 CAP45 scaffold	WT	N143D	N147D	N156D	N160Q	N192D
PG9	0.2	0.1	0.1	4.9	-	0.2
PG16	9.1	3.3	0.7	-	-	27.0

"-" indicates no binding or EC_{50}>50µg/mL

For 1FD6 CAP45 scaffold, a combination of multiple glycosylation mutants was also tested. N156D/N160Q did not bind PG9 nor PG16. N143D/N147D/N192D bound PG9 with an EC_{50} of 0.1 µg/ml and PG16 with an EC_{50} of 15.1 µg/ml.

ELISA assay with purified protein:
WT and site mutated 1JO8 ZM109 V1V2 proteins produced in 293F cell (10mg/ swainsonine) in PBS (pH 7.4) at 2µg/ml were used to coat plates for 2 hours at room temperature (RT). The plates were washed five times with 0.05% Tween 20 in PBS (PBS-T), blocked with 300 µl per well of blocking buffer (5% skim milk and 2% bovine albumin in PBS-T) for 1 hour at RT. 100 µl of each monoclonal antibodies 5-fold serially diluted in blocking buffer were added and incubated for 1 hour at RT. Horseradish peroxidase (HRP)-conjugated goat anti-human IgG (H+L) antibody (Jackson ImmunoResearch Laboratories Inc., West Grove, PA) at 1:5,000 was added for 1 hour at RT. The plates were washed five times with PBS-T and then developed using 3,3´,5,5´-tetramethylbenzidine (TMB) (Kirkegaard & Perry Laboratories) at RT for 10 min. The reaction was stopped by the addition of 100µl 1 N H2SO4 to each well. The readout was measured at a wavelength of 450nm. All samples were performed in duplicate.

ELISA assay with supernatant:
Culture supernatants from 293F cell (10mg/L, swainsonine) transfected with WT and site mutated 1FD6 CAP45 V1V2 were used to coat His grab plates (150µL/well) for overnight at 4 °C. 100 µL of each monoclonal antibodies 5-fold serially diluted in blocking buffer were added and incubated for 1 hour at RT. Horseradish peroxidase (HRP)-conjugated goat anti-human IgG (H+L) antibody (Jackson ImmunoResearch Laboratories Inc., West Grove, PA) at 1:5,000 was added for 1 hour at RT. The plates were washed five times with PBS-T and then developed using 3,3´,5,5´-tetramethylbenzidine (TMB) (Kirkegaard & Perry Laboratories) at RT for 10 min. The reaction was stopped by the addition of 100µL 1 N H2SO4 to each well. The readout was measured at a wavelength of 450nm. All samples were performed in duplicate.

Supplementary Table 12. PG9/PG16 heavy chain affinity maturation and CAP45/ZM109 V1V2 recognition*

Heavy PG9/16 Germline	Heavy PG9	Explanation	Heavy PG16 (modeled)	Explanation
SER 55	SER 55		MET 55	MET has larger surface than SER to interact with NAG 573
CDR H3 insertion	ASP 100	Contact glycans	ILE 100	ILE might clash with NAG 561
CDR H3 insertion	ARG 100B	Contact glycans/peptide	HIS 100B	Contact glycans/peptide
CDR H3 insertion	GLY 100D	Contact peptide	ASP 100D	Contact peptide
CDR H3 insertion	TYR 100E	Contact peptide	VAL 100E	Contact peptide – VAL might have weaker interaction
CDR H3 insertion	ASN 100F	Contact peptide	LYS 100F	Contact peptide – LYS might disrupt binding
TRP 100K	TYR 100K	TYR introduces a hydrogen bond with NAG 573	ASN 100K	Polar more favorable than hydrophobic
SER 100L	ASP 100L	ASP introduces a hydrogen bond with ARG 168 of V1V2	ASP 100L	Same as PG9
TYR or THR 100P	ASN 100P	ASN introduces a hydrogen bond with MAN 566	ASN 100P	Same as PG9
TYR 100R	HIS 100R	TYR will clash with MAN 566 and HIS introduces a new hydrogen bond with MAN 565	HIS 100R	Same as PG9

*Residues for which the buried surface area is $<5Å^2$ were not considered. Residues interacting with ZM109 V1V2 or CAP45 V1V2 that are not affinity matured are not listed (these include heavy chain ASP53, TYS 100G, TYS 100H, ASP 100I, PHE 100J, TYR 100O and TYR 100Q).

Supplementary Table 13. PG9/PG16 light chain affinity maturation on CAP45/ZM109 V1V2 recognition*

Light PG9/PG16 Germline	Light PG9	Explanation	Light PG16 (Modeled)	Explanation
TYR 30	TYR 30		PHE 30	Unclear
ASN 31	GLU 31	Interaction is through main chain with MAN 565	ASP 31	Same as PG9
TYR 32	SER 32	TYR will clash with MAN 565 and possible loss of one hydrogen bond	SER 32	Same as PG9
GLU 50	ASP 50	Both GLU and ASP should interact	ASP 50	Same as PG9
ASN 53	LYS 53	ASN might lose interaction with MAN 565	HIS 53	Same as PG9
TYR 91	LEU 91	TYR will clash with heavy HIS 100R	LEU 91	Same as PG9
SER 95	ARG 95	ARG closer to MAN 566	SER 95	
LEU 96	ARG 96	ARG closer to MAN 566	ARG 96	Same as PG9

*Residues for which the buried surface area is <5Å^2 were not considered.

Supplementary Table 14. Structural effect of V1V2 mutations on PG9 neutralization

Residue	JR-CSF[1]		ConC[2]		Predicted Structural Effect
	Mutation	Fold IC_{50} Increase	Mutation	Fold IC_{50} Increase	
127	**V→A**	**30**	*NA*[3]		disruption of V1V2 hydrophobic core
134	N→A	5	*NA*		
156	**N→A**	**280**	*NA*		glycan-156 removal
158	**S→A**	**>2000**	S→A	0.9	glycan-156 removal
159	**F→A**	**>2000**	**F→A**	**11.2**	disruption of V1V2 hydrophobic core
160	**N→K**	**>2000**	**N→A**	**>1000**	glycan-160 removal
162	**T→A**	**>2000**	*NA*		glycan-160 removal
165	I→A	1	L→A	2	
166	R→A	2	R→A	0.5	
167	D→A	5	D→N	0.6	
168	K→A	1	K→A	0.1	
169	*NA*[3]		**K→E**	**>1000**	contact site, PG9 TYS 100G proximal
171	K→A	1	K→A	5.9	
172	E→A	1	*NA*		
173	**Y→A**	**1400**	*NA*		destabilization of glycan-156 position
176	**F→A**	**>5000**	*NA*		disruption of V1V2 hydrophobic core
177	Y→A	1	*NA*		
179	L→A	1	*NA*		
180	D→A	1	*NA*		
181	**V→A**	**200**	**I→A**	**13.2**	unknown: residue not seen in structures
182	V→A	1	*NA*		
184	I→A	1	*NA*		
185	D→A	1	*NA*		
188	N→A	3	*NA*		
190	T→A	2	*NA*		

Effect on neutralization of mutants is shown in two contexts, JR-CSF and ConC. Mutations with greater than ten-fold increase in IC_{50} values are in bold.

[1]Data obtained from (Walker *et al*., Science, 2009)

[2]Data obtained from (Moore *et al*., J. Virol., 2011)

[3]*NA*, Data not available

Supplementary Table 15. Neutralization activity of PG9, PG16, VRC01, 2F5 and 2G12 against a cross-clade panel of 178 pseudoviruses (IC_{50})

		% of Total Strains Neutralized					% of Strains Neutralized									
							IC50 <1ug/ml					IC50 >1 and <50ug/ml				
Clade	**# VS***	**PG9**	**PG16**	**VRC01**	**2F5**	**2G12**	**PG9**	**PG16**	**VRC01**	**2F5**	**2G12**	**PG9**	**PG16**	**VRC01**	**2F5**	**2G12**
A	27	89	89	100	85	30	92	92	100	26	13	8	8	0	74	88
AC	4	100	100	50	75	25	100	100	100	0	0	0	0	0	100	100
ACD	2	50	50	100	100	0	100	100	100	50	0	0	0	0	50	0
AD	1	100	100	100	100	0	0	0	100	0	0	100	100	0	100	0
AE	16	88	81	94	94	0	86	92	80	60	0	14	8	20	40	0
AG	16	94	94	81	69	31	87	73	85	0	40	13	27	15	100	60
B	39	59	56	92	82	64	78	68	81	31	48	22	32	19	69	52
BC	7	100	100	100	14	14	71	71	86	0	100	29	29	14	100	0
C	53	81	75	85	9	6	84	83	80	20	33	16	18	20	80	67
CD	3	67	67	67	100	33	100	100	100	0	0	0	0	0	100	100
D	9	56	22	89	67	44	60	50	63	33	25	40	50	38	67	75
G	1	0	0	0	0	0	0	0	0	0	0	0	0	0	0	0
Total	178	78	74	89	57	27	83	81	84	28	38	17	19	16	72	63

*VS: Viral strains

Neutralization was measured using single-round-of-infection HIV-1 Env-pseudoviruses and TZM-bl target cells, as described previously (Wu et al., Science, 2010; Li et al., J.Virol., 2005; Seaman et al., J. Virol., 2010). Neutralization curves were fit by nonlinear regression using a 5-parameter hill slope equation as previously described (Li et al., J.Virol., 2005). The 50% and 80% inhibitory concentrations (IC_{50} and IC_{80}) were reported as the antibody concentrations required to inhibit infection by 50% and 80%, respectively.

Supplementary Table 16. Neutralization activity of mAbs against a cross-clade panel of 178 pseudoviruses (IC_{50})

Virus ID	Clade	VRC01	PG9	PG16	2F5	2G12
0260.v5.c36	A	0.529	2.18	2.10	>50	>50
0330.v4.c3	A	0.064	0.018	0.006	14.6	1.04
0439.v5.c1	A	0.052	>50	>50	4.43	>50
3415.v1.c1	A	0.092	0.149	0.036	43.9	1.32
3718.v3.c11	A	0.218	0.050	0.019	3.88	>50
398-F1_F6_20	A	0.058	>50	>50	0.280	32.2
BB201.B42	A	0.343	0.014	0.003	2.92	0.421
BB539.2B13	A	0.094	0.106	0.012	0.136	>50
BI369.9A	A	0.149	0.029	0.007	0.249	1.62
BS208.B1	A	0.029	0.031	0.004	1.10	>50
KER2008.12	A	0.563	0.017	0.006	6.98	10.7
KER2018.11	A	0.070	0.001	<0.0006	2.01	>50
KNH1209.18	A	0.087	0.367	0.678	2.24	1.45
MB201.A1	A	0.237	0.024	0.001	0.436	>50
MB539.2B7	A	0.544	0.058	0.025	2.49	>50
MI369.A5	A	0.162	0.058	0.011	1.44	5.09
MS208.A1	A	0.147	0.071	0.047	1.10	>50
Q168.a2	A	0.140	0.106	0.031	7.83	>50
Q23.17	A	0.086	0.007	0.002	10.8	>50
Q259.17	A	0.051	0.045	0.028	16.1	>50
Q461.e2	A	0.410	3.01	4.11	13.4	>50
Q769.d22	A	0.015	0.007	0.010	0.609	>50
Q769.h5	A	0.014	0.002	0.002	>50	>50
Q842.d12	A	0.006	0.005	0.001	>50	>50
QH209.14M.A2	A	0.024	>50	>50	>50	>50
RW020.2	A	0.303	0.103	0.070	7.55	>50
UG037.8	A	0.035	0.021	0.001	0.202	>50
3301_V1_C24	AC	0.084	0.281	<0.023	>50	>50
3589_V1_C4	AC	0.073	0.025	0.728	6.99	1.68
6540.v4.c1	AC	>50	0.035	0.017	40.0	>50
6545_V4_C1	AC	>50	0.095	0.068	26.0	>50
0815_V3_C3	ACD	0.036	>50	>50	7.37	>50
6095_V1_C10	ACD	0.464	0.242	<0.023	0.147	>50
3468_V1_C12	AD	0.040	2.09	2.38	3.51	>50
620345.c1	AE	>50	0.393	>50	0.455	>50
C1080.c3	AE	1.50	0.004	0.001	0.056	>50
C2101.c1	AE	0.097	0.026	0.009	0.344	>50
C3347.c11	AE	0.037	0.038	0.006	0.051	>50
C4118.09	AE	0.110	0.037	0.021	2.49	>50
CNE3	AE	3.56	0.079	0.173	6.79	>50
CNE5	AE	0.228	<0.023	<0.023	9.70	>50
CNE55	AE	0.292	0.146	1.37	1.49	>50
CNE56	AE	0.442	>50	>50	0.974	>50
CNE59	AE	0.516	0.091	0.113	0.029	>50
M02138	AE	0.742	0.122	0.022	0.023	>50
R1166.c1	AE	1.77	1.55	0.587	2.56	>50
R2184.c4	AE	0.052	0.20	0.280	1.73	>50
R3265.c6	AE	0.731	1.30	0.036	>50	>50
TH966.8	AE	0.331	0.042	0.008	0.182	>50
TH976.17	AE	0.066	>50	>50	0.131	>50

Supplementary Table 16 (cont'd). Neutralization activity of mAbs against a cross-clade panel of 178 pseudoviruses (IC_{50})

Virus ID	Clade	VRC01	PG9	PG16	2F5	2G12
235-47	AG	0.049	0.322	0.246	>50	0.519
242-14	AG	>50	0.025	<0.023	1.06	>50
263-8	AG	0.119	0.353	1.31	>50	6.84
269-12	AG	0.163	1.52	0.281	>50	>50
271-11	AG	0.052	0.097	0.102	13.2	>50
928-28	AG	0.378	0.060	0.023	1.04	>50
DJ263.8	AG	0.072	0.100	0.048	>50	0.721
T250-4	AG	>50	<0.0006	<0.0006	2.93	15.6
T251-18	AG	3.58	>50	10.5	30.5	9.22
T253-11	AG	0.265	0.127	4.44	4.27	>50
T255-34	AG	0.252	0.015	0.005	>50	>50
T257-31	AG	1.68	0.020	0.003	5.46	>50
T266-60	AG	0.353	24.0	>50	8.04	>50
T278-50	AG	>50	0.913	1.13	4.27	>50
T280-5	AG	0.017	0.379	0.233	4.30	>50
T33-7	AG	<0.023	<0.023	<0.023	10.0	>50
3988.25	B	2.10	0.010	0.002	>50	0.251
5768.04	B	0.099	0.073	0.020	0.139	1.44
6101.10	B	0.104	>50	>50	>50	>50
6535.3	B	2.16	0.465	>50	4.90	3.43
7165.18	B	>50	>50	>50	1.35	0.840
89.6.DG	B	0.460	>50	>50	1.514	0.528
AC10.29	B	1.43	0.078	<0.023	0.975	>50
ADA.DG	B	0.424	0.342	0.023	0.271	9.51
Bal.01	B	0.102	0.052	8.00	4.13	0.203
BaL.26	B	0.047	0.034	0.136	3.16	0.628
BG1168.01	B	0.449	>50	>50	1.35	>50
BL01.DG	B	>50	>50	>50	6.02	5.27
BR07.DG	B	1.67	>50	>50	0.675	3.20
BX08_16	B	0.281	0.024	0.062	2.79	5.41
CAAN.A2	B	1.06	13.0	7.43	11.6	>50
HO86.8	B	>50	0.014	0.001	0.049	>50
HT593.1	B	0.438	0.271	0.153	0.172	6.83
HXB2.DG	B	0.040	0.553	>50	0.040	1.01
JRCSF.JB	B	0.234	0.003	0.002	9.45	0.857
JRFL.JB	B	0.033	>50	>50	7.84	1.76
MN.3	B	0.033	>50	>50	<0.023	0.213
PVO.04	B	0.386	6.24	19.8	>50	1.50
QH0515.01	B	0.52	>50	>50	0.3	0.039
QH0692.42	B	1.16	>50	>50	2.22	4.05
REJO.67	B	0.045	0.005	0.005	0.300	>50
RHPA.7	B	0.047	>50	1.32	23.2	>50
SC422.8	B	0.132	0.535	1.20	1.34	7.82
SF162.LS	B	0.237	>50	>50	2.47	0.313
SS1196.01	B	0.276	0.293	0.069	25.3	17.0
THRO.18	B	4.42	15.0	0.975	>50	>50
TRJO.58	B	0.079	0.246	0.393	>50	>50
TRO.11	B	0.343	41.5	4.86	>50	0.209
WITO.33	B	0.112	<0.023	<0.023	2.29	0.887
YU2.DG	B	0.055	3.69	0.041	>50	>50
CNE10	B	0.776	0.243	9.17	1.10	0.103
CNE12	B	0.785	>50	>50	5.02	>50
CNE14	B	0.389	>50	>50	5.68	>50
CNE4	B	0.871	>50	>50	1.77	>50

Supplementary Table 16 (cont'd). Neutralization activity of mAbs against a cross-clade panel of 178 pseudoviruses (IC_{50})

Virus ID	Clade	VRC01	PG9	PG16	2F5	2G12
CNE57	B	0.535	>50	>50	1.09	>50
CH038.12	BC	0.379	0.500	49.0	>50	0.031
CH070.1	BC	18.7	0.006	0.002	>50	>50
CH117.4	BC	0.059	0.008	0.005	>50	>50
CH181.12	BC	0.540	0.008	0.002	>50	>50
CNE15	BC	0.080	<0.023	<0.023	>50	>50
CNE7	BC	0.540	1.66	0.393	1.13	>50
CNE40	BC	0.425	1.16	49.0	>50	>50
286.36	C	0.103	0.071	0.005	>50	>50
288.38	C	1.52	3.14	0.186	>50	45.9
0013095-2.11	C	0.142	<0.023	<0.023	>50	>50
001428-2.42	C	<0.023	<0.023	<0.023	>50	>50
0077_V1.C16	C	1.04	0.091	<0.023	>50	>50
00836-2.5	C	0.128	49.0	>50	>50	>50
16055-2.3	C	0.105	0.014	0.005	>50	>50
16845-2.22	C	2.41	2.38	27.8	>50	>50
16936-2.21	C	0.109	>50	>50	>50	>50
25710-2.43	C	0.545	0.038	<0.023	>50	>50
25711-2.4	C	0.712	1.50	0.037	44.8	>50
25925-2.22	C	0.559	<0.023	<0.023	>50	>50
26191-2.48	C	0.195	0.142	1.95	>50	>50
3168.V4.C10	C	0.131	0.162	0.037	23.1	>50
3637.V5.C3	C	4.09	>50	>50	>50	>50
3873.V1.C24	C	0.954	>50	12.2	>50	>50
6322.V4.C1	C	>50	>50	>50	>50	>50
6471.V1.C16	C	>50	>50	>50	>50	>50
6631.V3.C10	C	>50	>50	>50	>50	>50
6644.V2.C33	C	0.164	0.033	35.3	0.219	>50
6785.V5.C14	C	0.332	<0.023	<0.023	>50	>50
96ZM651.02	C	0.525	>50	>50	>50	>50
BR025.9	C	0.271	0.044	0.009	>50	0.236
CAP210.E8	C	>50	0.087	<0.023	>50	>50
CAP244.D3	C	0.857	0.088	<0.023	>50	>50
CAP45.G3	C	9.47	<0.023	<0.023	>50	>50
CNE30	C	0.927	>50	>50	>50	>50
CNE31	C	0.962	13.5	2.51	>50	>50
CNE53	C	0.108	0.147	>50	>50	>50
CNE58	C	0.124	<0.023	<0.023	>50	>50
DU123.06	C	13.6	0.091	<0.023	>50	>50
DU151.02	C	7.70	<0.023	<0.023	>50	>50
DU156.12	C	0.082	<0.023	<0.023	>50	>50
DU172.17	C	>50	0.262	0.030	>50	>50
DU422.01	C	>50	0.303	<0.023	>50	>50
MW965.26	C	0.038	1.99	0.961	>50	>50
SO18.18	C	0.071	0.061	0.023	>50	>50
TV1.29	C	>50	0.008	0.002	3.29	13.4
TZA125.17	C	>50	0.231	0.024	>50	>50
TZBD.02	C	0.072	0.266	0.025	>50	>50
ZA012.29	C	0.250	27.0	0.631	>50	>50
ZM106.9	C	0.248	0.639	1.10	>50	>50
ZM109.4	C	0.134	0.106	4.93	>50	>50
ZM135.10a	C	1.28	>50	>50	>50	>50
ZM146.7	C	0.460	0.635	0.767	>50	>50
ZM176.66	C	0.038	0.007	0.002	>50	>50

Supplementary Table 16 (cont'd). Neutralization activity of mAbs against a cross-clade panel of 178 pseudoviruses (IC_{50})

Virus ID	Clade	VRC01	PG9	PG16	2F5	2G12
ZM197.7	C	0.624	0.414	0.650	35.7	>50
ZM214.15	C	0.881	>50	>50	>50	>50
ZM215.8	C	0.276	<0.023	>50	>50	>50
ZM233.6	C	4.25	<0.023	<0.023	>50	>50
ZM249.1	C	0.082	0.033	0.073	>50	>50
ZM53.12	C	0.839	0.041	<0.023	>50	>50
ZM55.28a	C	0.144	0.571	>50	>50	>50
3326.V4.C3	CD	0.073	<0.023	<0.023	19.6	>50
3337.V2.C6	CD	0.063	>50	>50	4.63	>50
3817.v2.c59	CD	>50	0.007	0.006	6.86	2.70
231965.c1	D	0.487	1.51	4.72	18.6	>50
247-23	D	24.2	0.195	>50	1.95	>50
3016.v5.c45	D	0.111	0.286	>50	0.765	>50
57128.vrc15	D	>50	0.104	0.162	>50	1.72
6405.v4.c34	D	2.63	>50	>50	7.51	14.8
A03349M1.vrc4a	D	4.66	>50	>50	>50	>50
NKU3006.ec1	D	0.506	>50	>50	1.10	>50
UG021.16	D	0.266	>50	>50	>50	2.12
UG024.2	D	0.106	3.94	>50	0.029	0.162
X2088_c9	G	>50	>50	>50	>50	>50
SIVmac251.30.SG3	NA	>50	>50	>50	>50	>50
SVA.MLV	NA	>50	>50	>50	>50	>50

IC_{50}<1µg/mL are shown in red; 1< IC_{50}<15µg/mL are shown in yellow;
15< IC_{50}<50 µg/mL are shown in green.

Supplementary Table 17. Neutralization activity of mAbs against a cross-clade panel of 178 pseudoviruses (IC_{80})

Virus ID	Clade	VRC01	PG9	PG16	2F5	2G12
0260.v5.c36	A	1.48	22.8	>50	>50	>50
0330.v4.c3	A	0.231	0.083	0.027	>50	13.6
0439.v5.c1	A	0.236	>50	>50	48.4	>50
3415.v1.c1	A	0.256	0.770	0.342	>50	5.84
3718.v3.c11	A	4.99	0.202	0.102	25.7	>50
398-F1_F6_20	A	0.320	>50	>50	>50	>50
BB201.B42	A	1.11	0.046	0.008	20.1	3.04
BB539.2B13	A	0.330	0.422	0.062	1.59	>50
BI369.9A	A	0.657	0.151	0.037	5.57	9.75
BS208.B1	A	0.104	0.098	0.012	9.87	>50
KER2008.12	A	1.74	0.085	0.046	44.4	>50
KER2018.11	A	0.40	0.004	0.002	19.1	>50
KNH1209.18	A	0.299	>50	>50	16.3	6.86
MB201.A1	A	0.478	0.193	0.019	5.44	>50
MB539.2B7	A	1.48	0.383	0.205	18.8	>50
MI369.A5	A	0.769	0.364	0.082	14.4	49.2
MS208.A1	A	0.668	0.589	31.8	4.88	>50
Q168.a2	A	0.374	0.342	0.106	>50	>50
Q23.17	A	0.252	0.020	0.004	38.6	>50
Q259.17	A	0.252	0.229	0.717	34.6	>50
Q461.e2	A	1.31	29.9	>50	31.4	>50
Q769.d22	A	0.074	0.033	11.0	9.52	>50
Q769.h5	A	0.070	0.007	0.020	>50	>50
Q842.d12	A	0.020	0.021	0.006	>50	>50
QH209.14M.A2	A	0.078	>50	>50	>50	>50
RW020.2	A	0.868	0.622	3.51	32.1	>50
UG037.8	A	0.130	0.085	0.004	1.21	>50
3301_V1_C24	AC	0.188	1.51	0.397	>50	>50
3589_V1_C4	AC	0.184	0.102	37.8	27.3	9.18
6540.v4.c1	AC	>50	0.213	0.154	no fit	>50
6545_V4_C1	AC	>50	0.315	0.562	>50	>50
0815_V3_C3	ACD	0.074	>50	>50	27.6	>50
6095_V1_C10	ACD	1.50	2.25	0.443	0.660	>50
3468_V1_C12	AD	0.121	>50	>50	14.6	>50
620345.c1	AE	>50	>50	>50	7.58	>50
C1080.c3	AE	9.33	0.011	0.004	2.84	>50
C2101.c1	AE	0.558	0.289	0.069	>50	>50
C3347.c11	AE	0.198	0.168	0.031	1.20	>50
C4118.09	AE	0.574	0.205	0.240	>50	>50
CNE3	AE	>50	1.12	>50	27.8	>50
CNE5	AE	0.788	<0.023	<0.023	18.8	>50
CNE55	AE	0.891	1.32	>50	15.5	>50
CNE56	AE	1.69	>50	>50	3.82	>50
CNE59	AE	1.68	0.465	>50	0.230	>50
M02138	AE	1.85	1.36	0.810	0.221	>50
R1166.c1	AE	7.05	9.24	12.5	20.3	>50
R2184.c4	AE	0.237	1.75	>50	18.1	>50
R3265.c6	AE	4.28	9.80	0.691	>50	>50
TH966.8	AE	1.24	0.183	0.030	2.66	>50
TH976.17	AE	0.444	>50	>50	3.28	>50
235-47	AG	0.139	1.08	3.490	>50	1.64
242-14	AG	>50	0.112	0.175	5.65	>50
263-8	AG	0.373	1.46	>50	>50	48.1

Supplementary Table 17 (cont'd). Neutralization activity of mAbs against a cross-clade panel of 178 pseudoviruses (IC_{80})

Virus ID	Clade	VRC01	PG9	PG16	2F5	2G12
269-12	AG	0.404	5.73	1.44	>50	>50
271-11	AG	0.200	1.41	>50	>50	>50
928-28	AG	0.960	0.301	0.249	5.71	>50
DJ263.8	AG	0.668	0.733	1.11	>50	4.27
T250-4	AG	>50	0.001	0.001	12.5	>50
T251-18	AG	10.2	>50	>50	>50	>50
T253-11	AG	0.772	1.72	>50	20.1	>50
T255-34	AG	0.978	0.114	0.079	>50	>50
T257-31	AG	5.80	0.075	0.021	23.6	>50
T266-60	AG	1.35	>50	>50	38.5	>50
T278-50	AG	>50	6.06	>50	34.3	>50
T280-5	AG	0.081	1.94	4.527	42.9	>50
T33-7	AG	<0.023	0.087	0.279	40.0	>50
3988.25	B	>50	0.091	0.080	>50	1.50
5768.04	B	0.942	1.32	>50	11.9	21.0
6101.10	B	0.330	>50	>50	>50	>50
6535.3	B	6.270	2.31	>50	28.4	37.1
7165.18	B	>50	>50	>50	25.3	4.07
89.6.DG	B	1.58	>50	>50	7.23	15.4
AC10.29	B	3.83	0.306	0.088	5.01	>50
ADA.DG	B	1.40	>50	0.458	4.18	>50
Bal.01	B	0.318	1.52	>50	33.1	>50
BaL.26	B	0.154	0.365	>50	25.4	7.77
BG1168.01	B	1.43	>50	>50	8.74	>50
BL01.DG	B	>50	>50	>50	29.0	>50
BR07.DG	B	4.67	>50	>50	4.82	>50
BX08_16	B	0.680	0.273	38.8	13.3	>50
CAAN.A2	B	2.63	>50	>50	43.1	>50
HO86.8	B	>50	0.125	0.020	2.33	>50
HT593.1	B	1.72	5.41	13.7	3.31	>50
HXB2.DG	B	0.077	10.2	>50	0.095	2.19
JRCSF.JB	B	0.804	0.009	0.015	42.1	5.39
JRFL.JB	B	0.117	>50	>50	33.6	8.50
MN.3	B	0.070	>50	>50	0.035	>50
PVO.04	B	0.990	37.1	>50	>50	10.0
QH0515.01	B	3.66	>50	>50	17.8	0.169
QH0692.42	B	3.00	>50	>50	11.6	16.6
REJO.67	B	0.207	0.080	0.400	8.71	>50
RHPA.7	B	0.155	>50	>50	>50	>50
SC422.8	B	0.331	38.6	>50	7.78	>50
SF162.LS	B	0.627	>50	>50	10.5	8.64
SS1196.01	B	0.650	3.08	2.90	>50	>50
THRO.18	B	15.1	>50	>50	>50	>50
TRJO.58	B	0.239	3.22	13.9	>50	>50
TRO.11	B	1.09	>50	>50	>50	0.489
WITO.33	B	0.267	0.030	<0.023	9.06	4.56
YU2.DG	B	0.149	>50	>50	>50	>50
CNE10	B	1.87	1.610	>50	5.04	0.339
CNE12	B	2.19	>50	>50	20.7	>50
CNE14	B	0.978	>50	>50	15.8	>50
CNE4	B	2.36	>50	>50	10.7	>50
CNE57	B	1.34	>50	>50	4.68	>50
CH038.12	BC	1.53	>50	>50	>50	0.155
CH070.1	BC	>50	0.024	0.013	>50	>50

Supplementary Table 17 (cont'd). Neutralization activity of mAbs against a cross-clade panel of 178 pseudoviruses (IC_{80})

Virus ID	Clade	VRC01	PG9	PG16	2F5	2G12
CH117.4	BC	0.334	0.030	0.028	>50	>50
CH181.12	BC	1.87	0.04	0.010	>50	>50
CNE15	BC	0.280	<0.023	<0.023	>50	>50
CNE7	BC	1.36	4.50	1.91	3.45	>50
CNE40	B'C	4.41	20.0	>50	>50	>50
286.36	C	0.379	0.385	0.018	>50	>50
288.38	C	5.86	>50	>50	>50	>50
0013095-2.11	C	0.319	0.061	0.149	>50	>50
001428-2.42	C	0.035	<0.023	<0.023	>50	>50
0077_V1_C16	C	3.65	0.343	0.075	>50	>50
00836-2.5	C	0.520	>50	>50	>50	>50
16055-2.3	C	0.365	0.060	0.016	>50	>50
16845-2.22	C	9.07	36.8	>50	>50	>50
16936-2.21	C	0.466	>50	>50	>50	>50
25710-2.43	C	1.56	0.179	0.120	>50	>50
25711-2.4	C	1.70	5.27	0.573	>50	>50
25925-2.22	C	1.39	0.063	0.025	>50	>50
26191-2.48	C	0.646	0.959	>50	>50	>50
3168.V4.C10	C	0.279	0.657	0.515	>50	>50
3637.V5.C3	C	11.0	>50	>50	>50	>50
3873.V1.C24	C	0.326	>50	>50	>50	>50
6322.V4.C1	C	>50	>50	>50	>50	>50
6471.V1.C16	C	>50	>50	>50	>50	>50
6631.V3.C10	C	>50	>50	>50	>50	>50
6644.V2.C33	C	0.528	0.120	>50	0.608	>50
6785.V5.C14	C	0.869	0.094	<0.023	>50	>50
96ZM651_02	C	1.94	>50	>50	>50	>50
BR025.9	C	1.08	0.215	0.049	>50	1.86
CAP210.E8	C	>50	0.501	0.882	>50	>50
CAP244.D3	C	2.36	0.362	0.058	>50	>50
CAP45.G3	C	>50	<0.023	<0.023	>50	>50
CNE30	C	2.59	>50	>50	>50	>50
CNE31	C	2.24	>50	>50	>50	>50
CNE53	C	0.280	0.809	>50	>50	>50
CNE58	C	0.313	0.068	<0.023	>50	>50
DU123.06	C	>50	0.477	0.163	>50	>50
DU151.02	C	>50	0.057	<0.023	>50	>50
DU156.12	C	0.244	0.143	<0.023	>50	>50
DU172.17	C	>50	0.899	0.134	>50	>50
DU422.01	C	>50	15.8	49.9	>50	>50
MW965.26	C	0.116	49.9	>50	>50	>50
SO18.18	C	0.166	0.227	0.136	>50	>50
TV1.29	C	>50	0.044	0.150	10.9	>50
TZA125.17	C	>50	1.21	0.719	>50	>50
TZBD.02	C	0.228	1.30	0.175	>50	>50
ZA012.29	C	0.828	>50	>50	>50	>50
ZM106.9	C	0.638	6.58	>50	>50	>50
ZM109.4	C	0.394	2.64	>50	>50	>50
ZM135.10a	C	6.16	>50	>50	>50	>50
ZM146.7	C	1.62	6.78	>50	>50	>50
ZM176.66	C	0.246	0.050	0.010	>50	>50
ZM197.7	C	1.55	1.92	6.67	>50	>50
ZM214.15	C	3.04	>50	>50	>50	>50
ZM215.8	C	0.833	0.228	>50	>50	>50

Supplementary Table 17 (cont'd). Neutralization activity of mAbs against a cross-clade panel of 178 pseudoviruses (IC_{80})

Virus ID	Clade	VRC01	PG9	PG16	2F5	2G12
ZM233.6	C	23.1	<0.023	<0.023	>50	>50
ZM249.1	C	0.242	0.408	9.23	>50	>50
ZM53.12	C	2.84	0.170	0.103	>50	>50
ZM55.28a	C	0.532	11.5	>50	>50	>50
3326_V4_C3	CD	15.2	0.111	0.221	>50	>50
3337_V2_C6	CD	0.133	>50	>50	22.2	>50
3817.v2.c59	CD	>50	0.028	0.051	48.1	29.7
231965.c1	D	1.55	>50	>50	>50	>50
247-23	D	>50	0.909	>50	16.2	>50
3016.v5.c45	D	0.341	>50	>50	12.0	>50
57128.vrc15	D	>50	0.665	>50	>50	13.4
6405.v4.c34	D	7.36	>50	>50	37.0	>50
A03349M1.vrc4a	D	28.1	>50	>50	>50	>50
NKU3006.ec1	D	1.78	>50	>50	26.5	>50
UG021.16	D	0.970	>50	>50	>50	>50
UG024.2	D	0.536	>50	>50	0.681	0.574
X2088_c9	G	>50	>50	>50	>50	>50
SIVmac251.30.SG3	NA	>50	>50	>50	>50	>50
SVA.MLV	NA	>50	>50	>50	>50	>50

IC_{80}<1µg/mL are shown in red; 1< IC_{80}<15µg/mL are shown in yellow;
15< IC_{80}<50 µg/mL are shown in green.

Supplementary Table 18. Data collection and refinement statistics for gp120-T13

	gp120-T13
Data collection	
Space group	$P4_3$
Cell dimensions	
a, *b*, *c* (Å)	122.42, 122.42, 178.41
α, β, γ (º)	
Resolution (Å)	50.0 – 6.00 (6.21-6.00)*
Mosaicity (º)	0.6
I/σI	14.4 (2.0)*
Completeness (%)	99.5 (99.8)*
Redundancy	3.8
Structure solution	
gp120 (PDB ID: 3HI1)	
Rotation (Euler) α, β, γ (º)	147.44, -100.52, 2.34
Translation vector (Å)	44.20, 62.84, -43.19
Fab (PDB ID: 1HZH)	
Rotation (Euler) α, β, γ (º)	62.81, -60.86, 43.98
Translation vector (Å)	258.09, 139.37, -93.15
Refinement (rigid body with no positional refinement)	
Resolution (Å)	50.0 – 6.00
No. reflections	6,435 (630)*
R_{work}/R_{free}	0.31/0.46

*****Values in parentheses are for highest-resolution shell.

Supplementary Table 19. Data collection and refinement statistics for unbound Fabs from V1V2-directed broadly neutralizing antibodies

	PG9 Fab	CH04 Fab	CH04H/CH02L Fab	CH04H/CH02L Fab	PGT145 Fab
Data collection					
Space group	P1	$P2_12_12_1$	$P4_32_12$	$P2_12_12_1$	$P4_12_12$
Cell dimensions					
a, *b*, *c* (Å)	71.59, 81.04, 91.70	73.36, 74.23, 183.57	86.20, 86.20, 185.68	70.61, 105.54, 163.97	118.73, 118.73, 101.18
α, β, γ (°)	107.2, 90.1, 108.0	90, 90, 90	90, 90, 90	90, 90, 90	90, 90, 90
Resolution (Å)	50.0-3.30 (3.42-3.30) *	50.0-1.90 (1.93-1.90)*	50.0-2.90 (3.00-2.90)*	50.0-2.90 (2.95-2.90)*	50.0-2.30 (2.40-2.30)*
R_{sym} or R_{merge}	0.12 (0.35)	0.13 (0.50)	0.14 (0.53)	0.11 (0.55)	0.09 (0.47)
$I / \sigma I$	7.4 (1.9)	15.1 (3.0)	14.2 (2.2)	13.1 (1.8)	19.1 (4.1)
Completeness (%)	89.2 (73.1)	99.9 (99.7)	97.9 (90.4)	82.7 (50.1)	99.2 (99.9)
Redundancy	1.7 (1.5)	6.9 (5.0)	6.8 (3.9)	5.3 (3.5)	8.4 (8.6)
Molecules/ASU	4	2	1	2	1
Refinement					
Resolution (Å)	38.5-3.28	39.7-1.90	30.5-2.89	32.4-2.91	50.0-2.30
No. reflections	24,997	78,886	15,976	22,836	32,692
R_{work} / R_{free}	21.4/24.9	19.6/23.8	22.1/26.8	21.5/24.5	19.1/22.6
No. atoms					
Protein	12,824	6,858	3,398	6,780	3,491
Ligand/ion	30	10	0	0	0
Water	0	624	38	22	353
B-factors					
Protein	125.0	38.7	68.9	87.3	24.3
Ligand/ion	162.2	24.1	-	-	-
Water	-	43.1	51	51	36.1
R.m.s. deviations					
Bond lengths (Å)	0.004	0.013	0.003	0.002	0.009
Bond angles (°)	0.90	1.39	0.72	0.58	1.20
PDB ID	3U36	3TCL	3U4B	3U46	3U1S

*Values in parentheses are for highest-resolution shell. Each data set was collected from a single crystal.

Supplementary Table 20. CH01-04 crystallization

	Heavy Chain			
Light Chain	**CH01 H**	**CH02 H**	**CH03 H**	**CH04 H**
CH01 L	Small crystals, not reproducible	Low yield (IgG)	Low yield (IgG)	No crystals
CH02 L	Low yield (IgG)	No crystals	Low yield (IgG)	**Two crystal forms, 2.9 Å resolution**
CH03 L	Needle like crystals, can reproduce but not optimize	No crystals	Small crystals, not reproducible	Crystals, not reproducible
CH04 L	Not Done	Not Done	Not Done	**Crystals, 1.9 Å resolution**

Supplementary Table 21. V1V2 and PG9 interface surface areas

	CAP45		ZM109	
	V1V2	PG9	V1V2	PG9
Total surface area (Å^2)	1611	1376	1299	1124
Glycan	69%	64%	60%	52%
B-*C* hairpin	31%	36%	40%	48%
Strand *B*	3%	7%	3%	8%
Connecting *B*-*C* loop	3%	5%	5%	5%
Strand *C*	25%	24%	31%	27%
Electrostatic (Å^2)	141	151	153	89
Sequence-independent (Å^2)	348	330	350	321

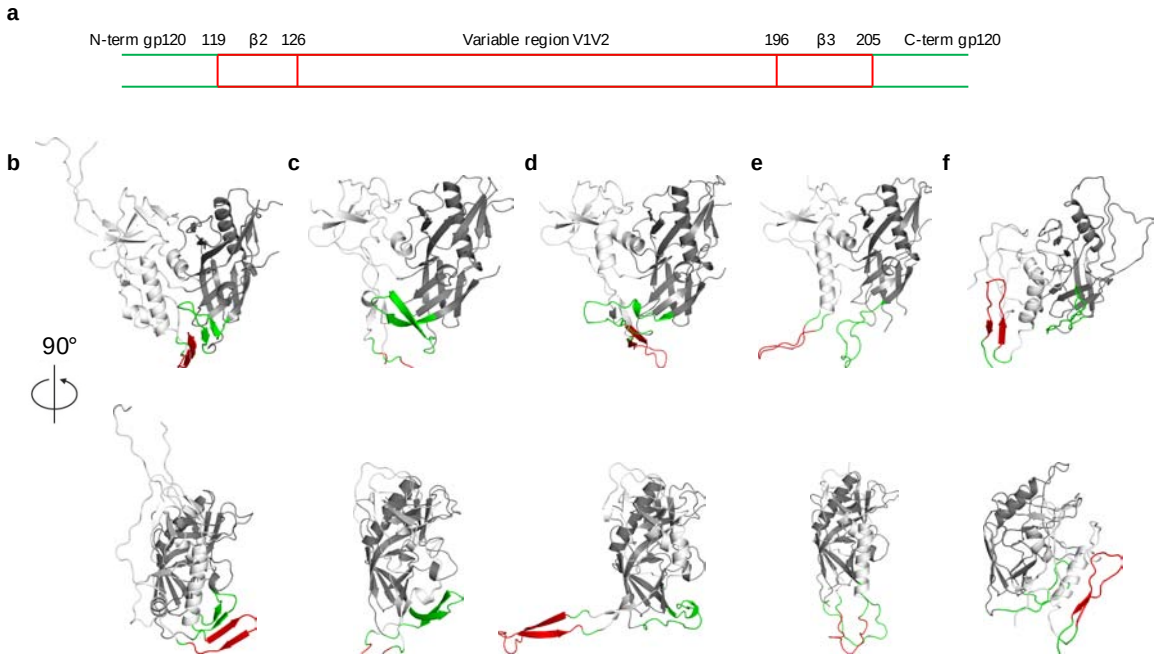

Supplementary Figure 1. V1V2 β-hairpin stubs in previously determined core structures of HIV-1 and SIV.
V1V2 residues (119-205 in HIV-1 HXB2 numbering and 103-215 in SIV numbering) are highlighted in red; in all cases, residues 128-194 of V1V2 were deleted from the crystallization construct and in some cases, the deletion was more extensive. **a,** Schematic of the bridging sheet and variable region V1V2, with the location of conserved cysteines at residues 119, 126, 196 and 205 highlighted. The V1V2 region has historically been defined as encompassing residues 119-205. Residues 119-127 and residues 195-205 have been defined crystallographically, and these form part of the "bridging sheet" region in the CD4-bound conformation of gp120, with the β2- and β3-strands of gp120 defining residues 119-123 and 199-203, respectively. **b,** 48d- and CD4-bound gp120. **c,** b12- bound. **d,** b13-bound. **e,** F105-bound. **f,** unliganded SIV core.

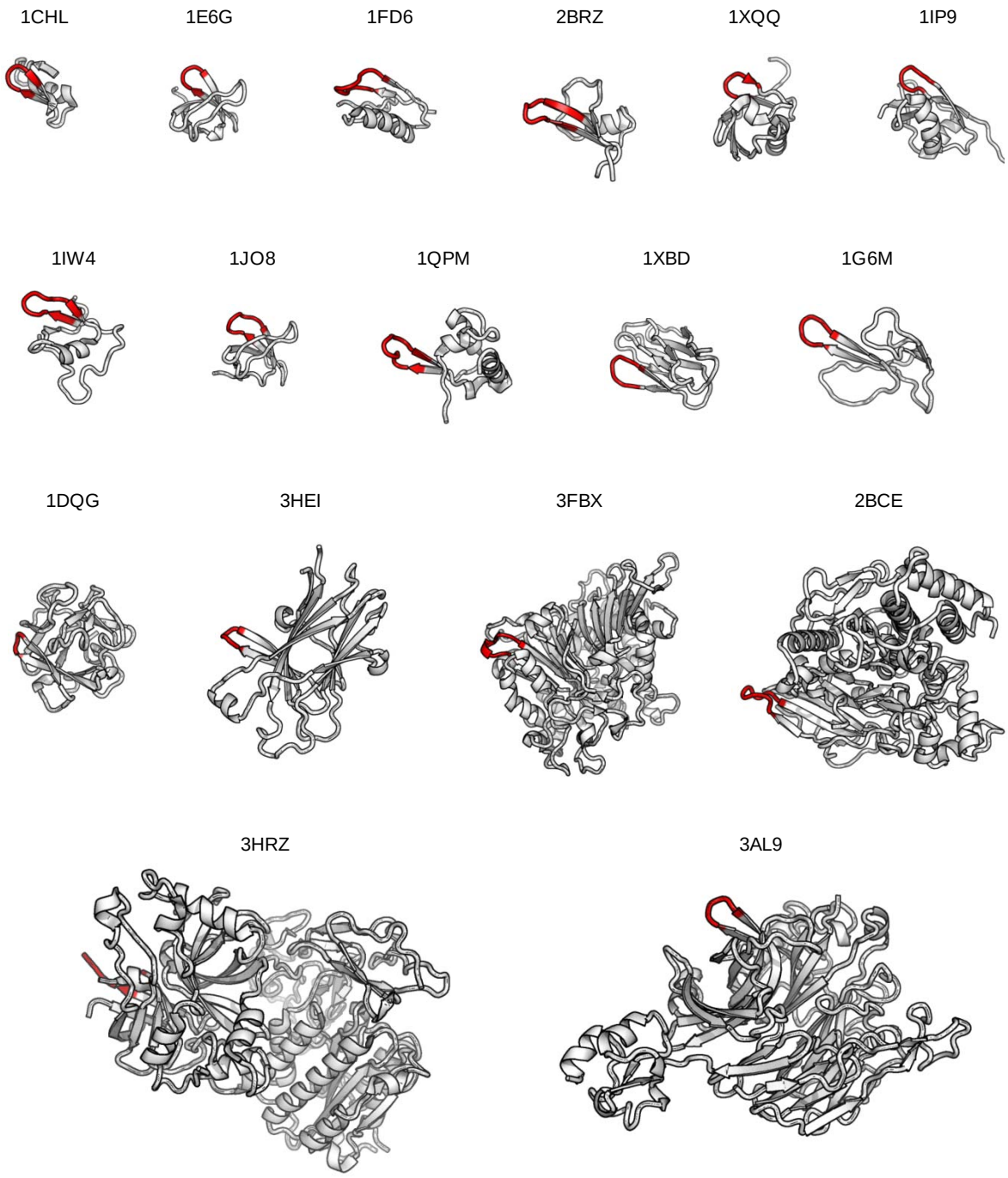

Supplementary Figure 2. Scaffold proteins used to host V1V2 regions.
Structures of the scaffold proteins before transplantation of the V1V2 region are shown as grey ribbon diagrams, with their PDB ID codes listed above. The red segment in each scaffold was removed for insertion of the V1V2 region.

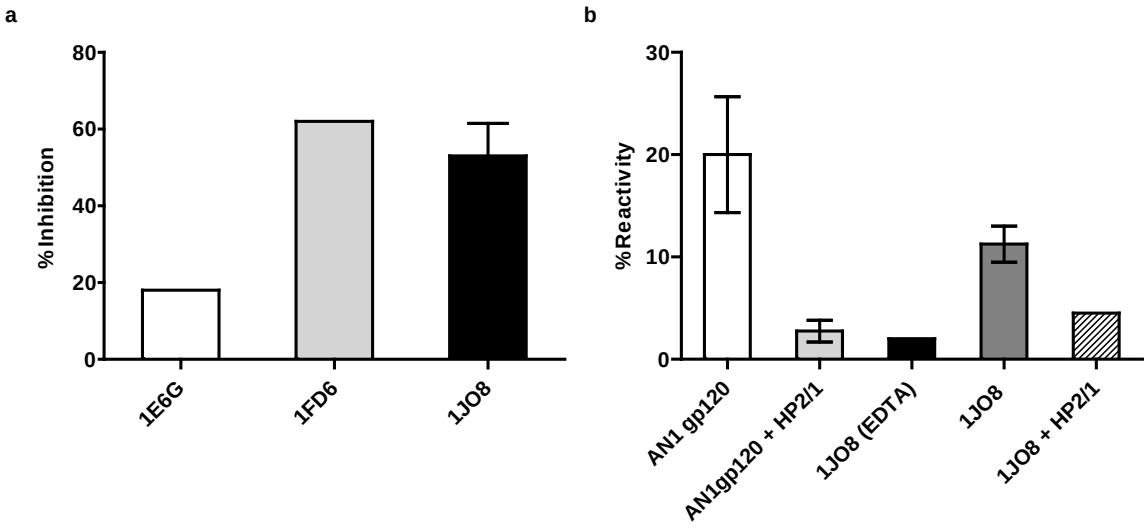

Supplementary Figure 3. HIV-1 gp120 V1V2 scaffolds interact with gut-homing receptor, integrin $\alpha_4\beta_7$. YU2 V1V2 scaffold proteins interaction with $\alpha_4\beta_7$ was studied by an indirect and direct binding assay. **a**, Indirect binding assay: % inhibition of AN1 gp120 binding to $\alpha_4\beta_7$ on CD4+ T cells by three YU2 V1V2 scaffold proteins (1JO8, 1E6G, 1FD6). In the competition assay, purified CD4+ T cells were preincubated with an anti-CD4 antibody (Leu3A) and YU2 V1V2 scaffold proteins in divalent cation containing buffer (1mM $MnCl_2$ and 100um $CaCl_2$) followed by the addition of biotin labeled ancestral gp120 (AN1 gp120). Mean fluorescence intensity (MFI) was measured to determine the extent of inhibition of AN1 gp120 binding to $\alpha_4\beta_7$ by the YU2 V1V2 scaffold proteins. This experiment was performed with 5-fold molar excess scaffold proteins over AN1 gp120. This initial competition assay indicated that two of the scaffolds, 1FD6A and 1JO8, provided the most pronounced inhibition of all scaffolds tested, therefore, a direct binding assay was performed with YU2 V1V2 1JO8. **b**, Direct binding assay: % reactivity of YU2 V1V2 1JO8 scaffold protein to $\alpha_4\beta_7$ on CD4+ T cells. The scaffold protein was biotinylated and used to bind directly to CD4+ T cells in the presence of Leu3A and divalent cations (1 mM $MnCl_2$ and 100 µM $CaCl_2$). Binding of AN1 gp120 and YU2 V1V2 1JO8 to CD4+ T cells is reduced to background levels in the presence of HP2/1, an anti α_4 antibody. Separate duplicate experiments were performed for each assay, and SD error bars are shown (except for 1JO8 binding to $\alpha_4\beta_7$ in EDTA containing buffer and its inhibition by HP2/1). Note that PG9 does not inhibit gp120 (subtype A/E) binding to $\alpha_4\beta_7$ in our assays.

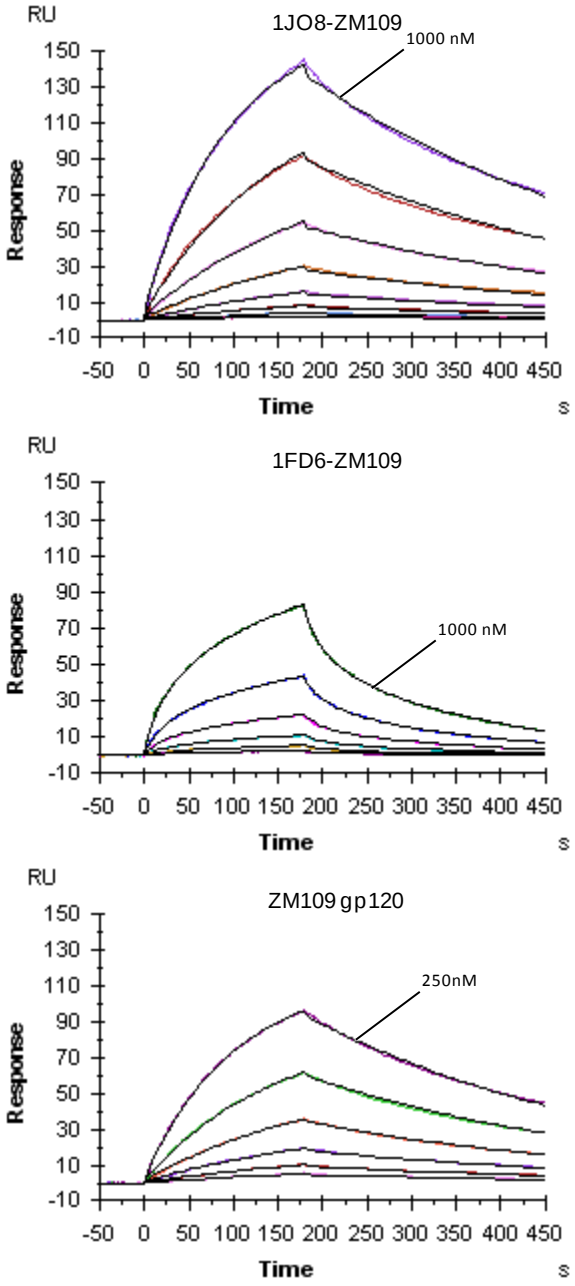

ka= 7.96E3 ± 21(1/Ms)
kd= 2.53E-3 ± 4.40E-6 (1/s)
K_D= 3.18E-7 ± 1.00E-9 (M)

Component 1: 29.0%
ka_1= 1.29E3 ± 20 (1/Ms)
kd_1= 5.14E-3 ± 1.00E-5 (1/s)
K_{D1}= 3.98E-6 ± 6.22E-08 (M)

Component 2: 71.0%
ka_2= 7.89E3 ± 260 (1/Ms)
kd_2= 4.47E-2 ± 3.50E-4 (1/s)
K_{D2}= 5.67-6 ± 1.92E-07 (M)

ka= 2.95E4 ± 65 (1/Ms)
kd= 2.85E-3 ± 3.6E-6 (1/s)
K_D= 9.68E-8 ± 2.46E-10 (M)

Supplementary Figure 4. Binding of HIV-1 ZM109 gp120 and V1V2 scaffolds to antibody PG9.
Surface-plasmon resonance sensorgrams with their respective fitted curves (black) are shown, with the highest concentration of each 2-fold dilution series labeled. The association and dissociation rates as well as the affinity values are shown to the right of the sensorgrams. In curves fitted with a heterogenous model, separate kinetics data are listed, along with contributing percentages for each component. Data were processed as described in Methods.

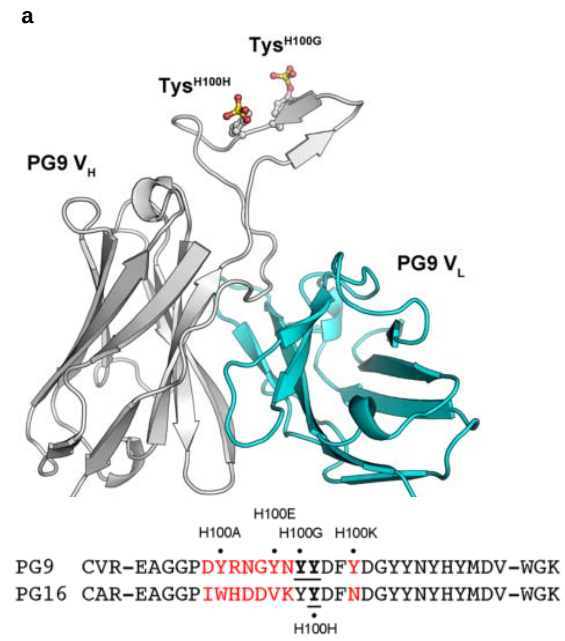

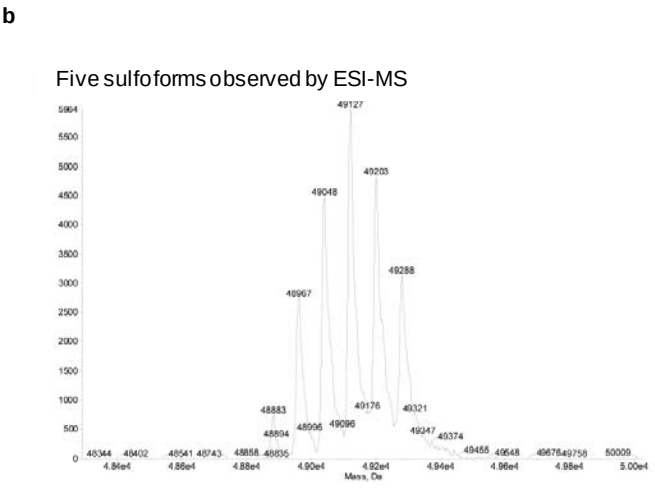

ESI-MS masses obtained for PG9 (HEK 293S GnTI -/-) and PG9$^{(N24T)}$ (HEK 293T) variants co-expressed with TPST-1.

	PG9		PG9$^{(N24T)}$		
	calc	obs	calc	obs	# sulfotyrosines
S5	50504	50527, 50529	49274	49288	5
S4	50425	50450, 50441	49195	40203	4
S3	50346	50357, 50356	49116	49127	3
S2	50267	50291, 50277	49037	49048	2
S1	50188	50194, 50195	48958	48967	1

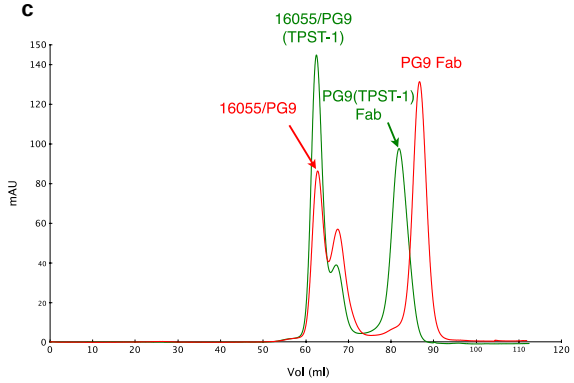

d

Neutralization potency of PG9 co-expressed with TPST-1 or in Sf9/baculovirus.

	PG9-NS	PG9-S1	PG9-S2	PG9-S3	PG9-S4	PG9-S5	IC50 (µg/ml)
PG9-S2 enriched			X				0.04
PG9-S enriched		X					0.8
PG9 (TPST-1) f39					X	X	0.04
PG9 (TPST-1) f42		X	X	X	X	X	n/d
PG9 (TPST-1) f43		X	X				0.08
PG9 (Sf9/baculovirus)	X						0.6

Supplementary Figure 5. PG9 tyrosine sulfate (TYS) characterization.
a, PG9 Fab has two sulfated tyrosines although there is some heterogeneity. **b,** Sulfation is controlled by tyrosyl protein sulfotransferase (TPST) and co-expression of TPST-1 promotes hypersulfation of PG9 (up to quintuple). Hypersulfated PG9 Fab was produced by co-expression of human tyrosyl protein sulfotransferase (TPST-1) in HEK 293T. Hyposulfated PG9 Fab was produced in Sf9 cells using a recombinant baculovirus, pFastBac Dual, expressing both the heavy and light chains under the control of the polyhedron and p10 promoters, respectively. Fabs were purified by anti-lambda affinity (CaptureSelect, BAC) and cation exchange using Mono S (GE HealthCare). Fractionation of PG9 sulfoforms was achieved by a shallow KCl gradient and individual fractions were characterized by electrospray time-of-flight mass spectrometry (ESI-TOF). **c,** Sulfation enhances PG9 association with gp120. Hypersulfated PG9 Fab (green, co-expressed with TPST-1) shows higher affinity for monomer than not hypersulfated PG9 Fab (red), however PG9 binary complex does not completely survive SEC. **d,** Effect of neutralization of hyper-sulfated PG9. Tyrosine to phenylalanine CDR H3 mutants (H100A, H100E, H100G, H100H, and H100K) were generated by the polymerase incomplete primer extension method (PIPE), expressed, purified, and fractionated as for wild-type.

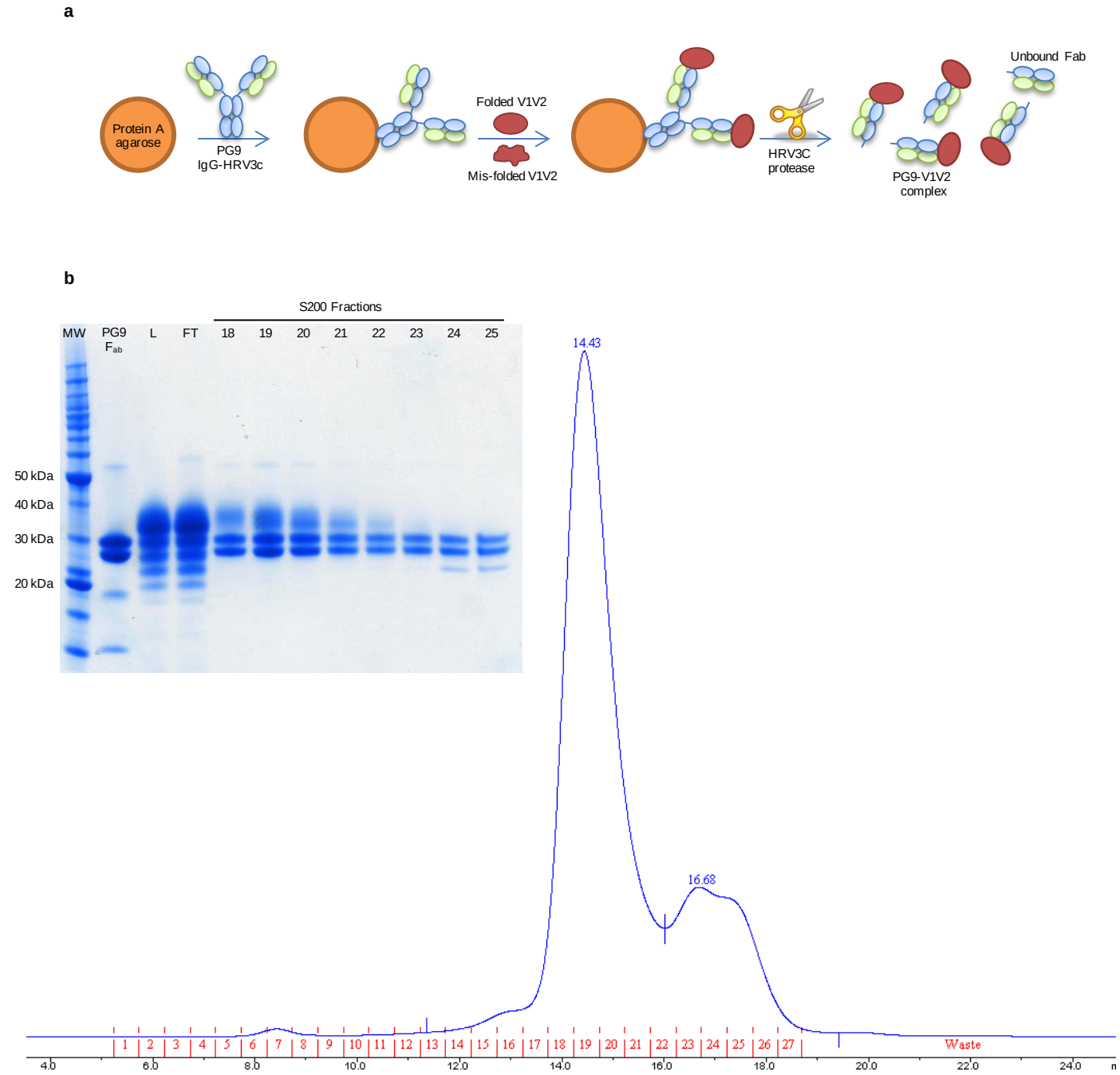

Supplementary Figure 6. On-column complex formation and purification.

a, Schematic of the on-column complex formation between PG9 and scaffolded V1V2s, as described in Methods. **b,** Gel filtration result of the elution shown in (**a**) for 1JO8 ZM109. A coomassie blue-stained SDS-PAGE gel is shown for fractions 18-25. MW=molecular weight standards. L=purified 1JO8 ZM109 before passage over the PG9-bound resin. FT=flow through of purified 1JO8 ZM109 after passage over the PG9-bound resin.

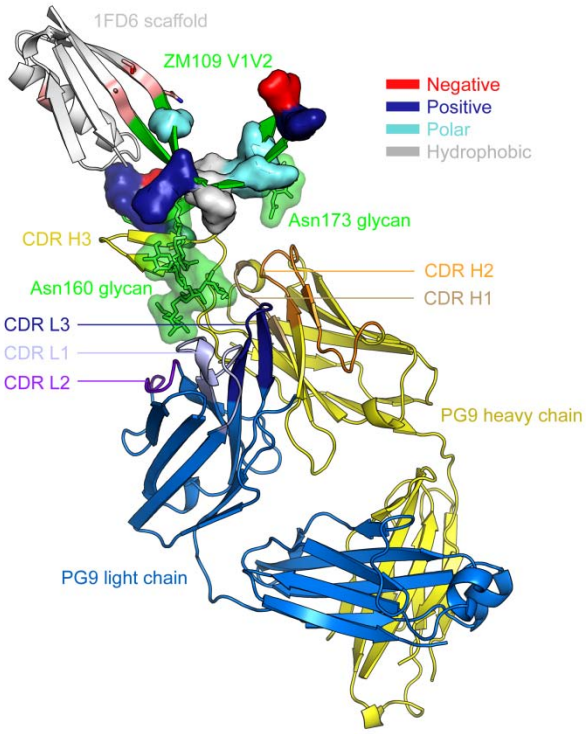

Supplementary Figure 7. Structure of PG9 in complex with the V1V2 region from HIV-1 strain ZM109. The PG9 heavy and light chains are shown as yellow and blue ribbons, respectively, with CDRs colored different shades. V1V2 residues 126-196 from HIV-1 strain ZM109 are shown as green ribbons, and attached glycans are shown as sticks with a transparent molecular surface. Residues that are different from the CAP45 strain (main text Fig 1) are shown as opaque molecular surfaces, colored according to chemical properties (red: negatively charged; blue: positively charged; cyan: polar; grey: hydrophobic). The 1FD6 scaffold is shown as white ribbons, with side chains shown as sticks and colored pink for those residues that were altered during the scaffolding process, including a Glu to Ala mutation that ablated IgG binding.

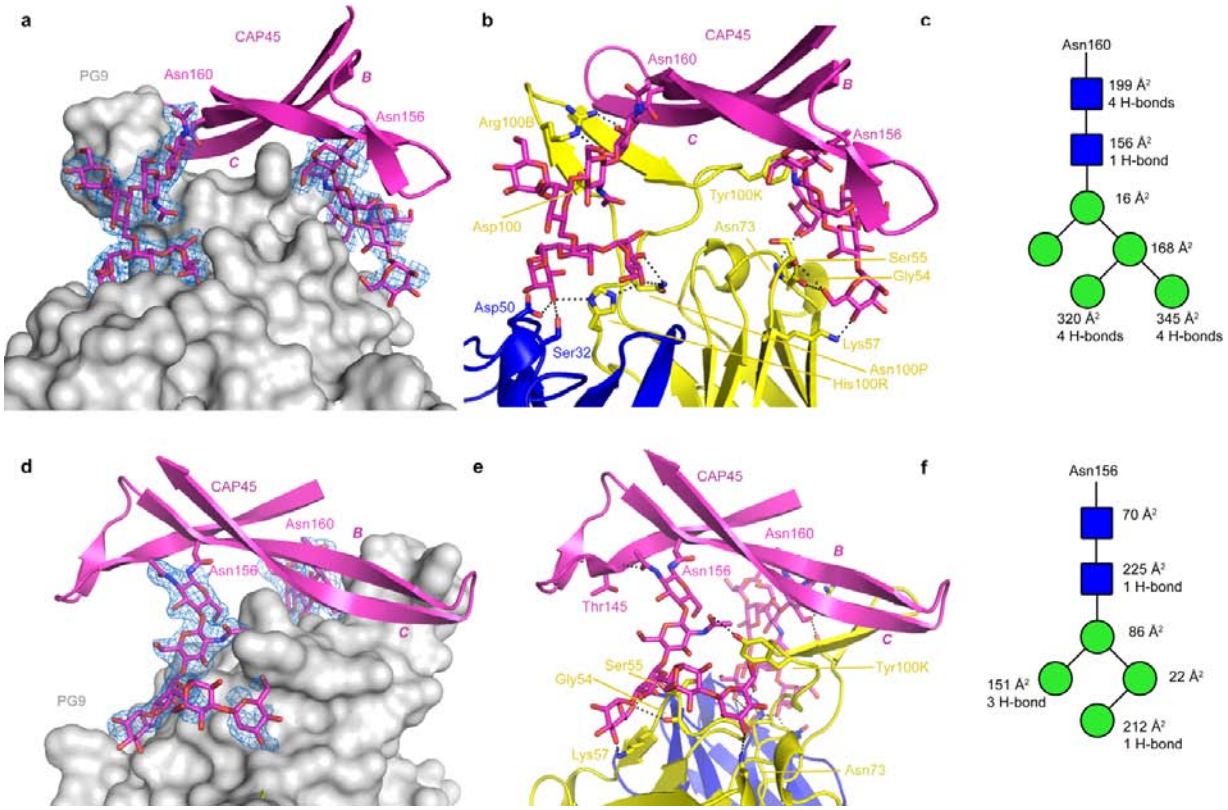

Supplementary Figure 8. Glycan recognition of CAP45 V1V2 by PG9.
PG9 recognizes the $Man_5GlcNAc_2$ glycan attached to Asn160 of CAP45 V1V2 through interactions analogous to those observed for ZM109. Additionally, the CAP45 V1V2 structure also reveals several interactions between PG9 and the Asn156-glycan. **a,** PG9 is represented as a grey molecular surface, and CAP45 V1V2 is shown as a ribbon diagram (magenta). Mannose and GlcNac residues are shown as sticks, as are the side-chains of Asn160 and Ans156. $2F_o$-F_c electron density contoured at 1σ is shown as a blue mesh. **b,** Ribbon representations of CAP45 V1V2 (magenta), PG9 heavy chain (yellow) and PG9 light chain (blue). Glycans and PG9 residues hydrogen-bonding to the glycans are shown as sticks. Nitrogen atoms are colored blue, oxygen atoms are colored red, and black dotted lines represent hydrogen bonds. **c,** Schematic of the $Man_5GlcNac_2$ moeity attached to Asn160. GlcNac is shown as blue squares, and mannose is shown as green circles. Hydrogen bonds to PG9 are listed to the right of the symbols, as is the total surface area buried at the interface between PG9 and each sugar. **d, e, f,** An orientation of the structure highlighting the interactions between PG9 and the Asn156-glycan of CAP45 V1V2 is presented in the lower three panels with representations corresponding to panels **a, b, c,** respectively.

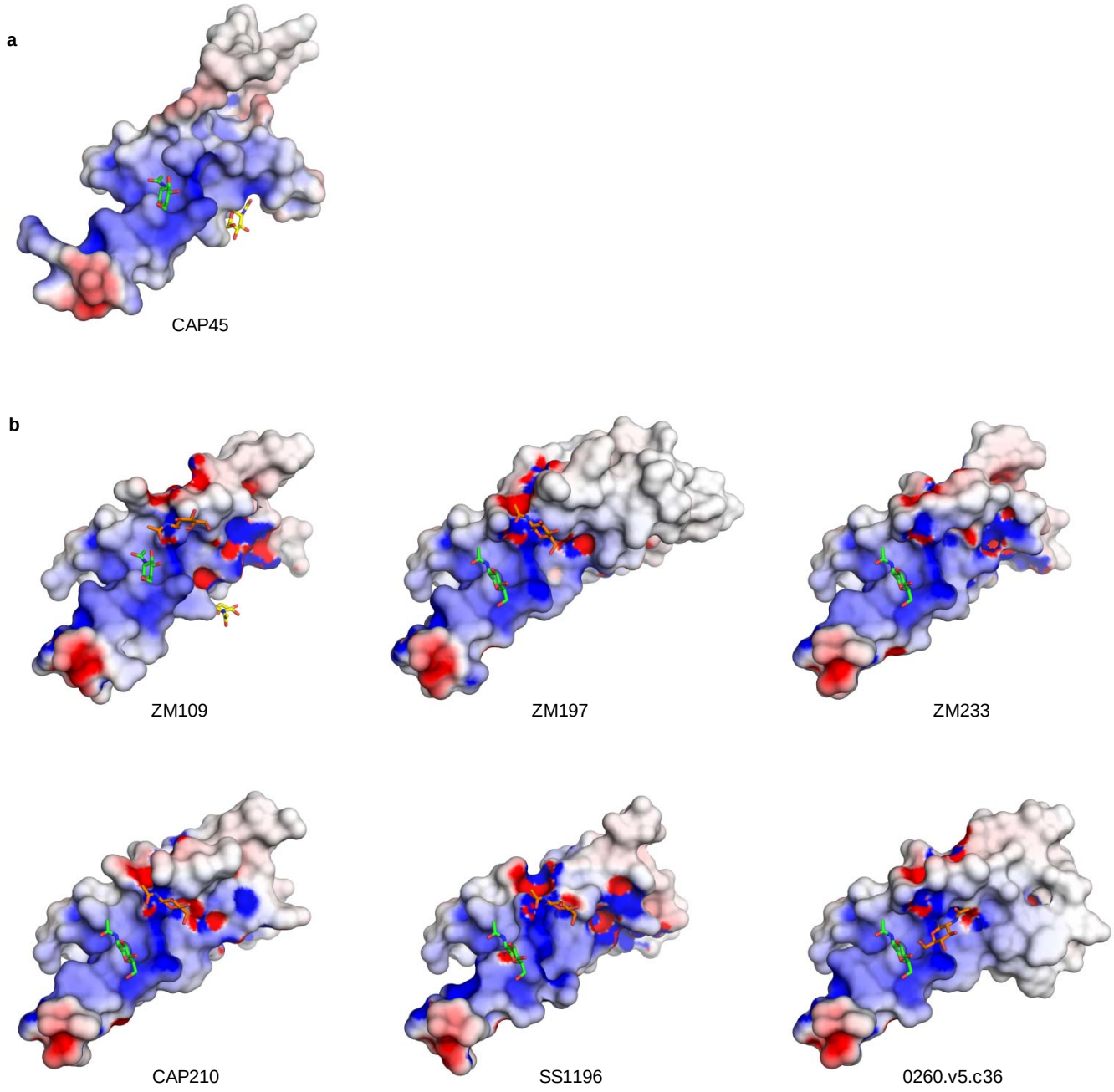

Supplementary Figure 9. HIV-1 strains with V1V2 regions lacking an *N*-linked glycan at position 156. Electrostatic surface potentials of V1V2, with modeled V1 and V2 loops. **a,** CAP45. **b,** ZM109 along with models of five additional strains lacking glycan 156. Coloring scale is blue to red, corresponding to positive and negative surface potentials, respectively. Potential glycosylation sites are shown for glycans 160 (green), 156/173 (yellow) and other glycosylation sites within strands *A-D* (orange). Glycans for the modeled V1 and V2 loops are not shown.

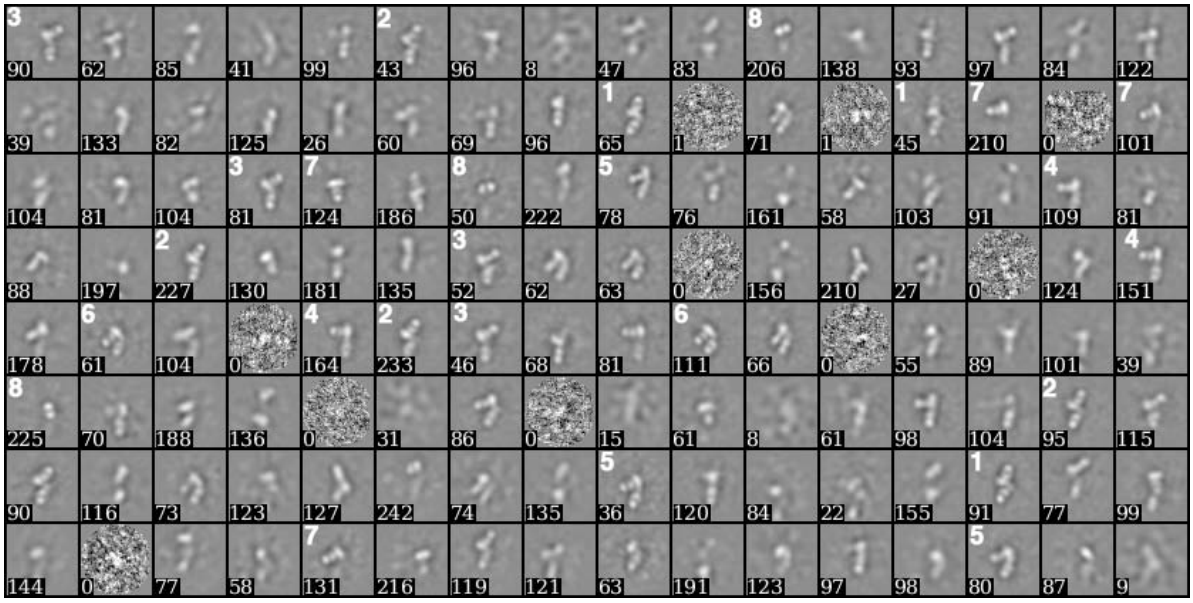

Supplementary Figure 10. Negative-stained reference-free 2D-class averages of the 128 classes calculated from untilted micrographs collected for the random conical tilt (RCT).

Class averages with white numbers in the top left were used to generate the RCT volumes. The white numbers represent the RCT volumes shown in Fig. 4b. Numbers in the lower left represent the total number of particles in each average. Reference free hierarchical class averaging within each class average produced indistinguishable results to the parent class average. An RCT volume was calculated from the appropriately combined class averages shown in this figure. RCTs were only calculated from class averages where the hole in the center of the T13 and PG9 Fabs were clearly visible. This hole in the center of the Fabs was used as a biophysical restraint to support the authenticity of the class averages.

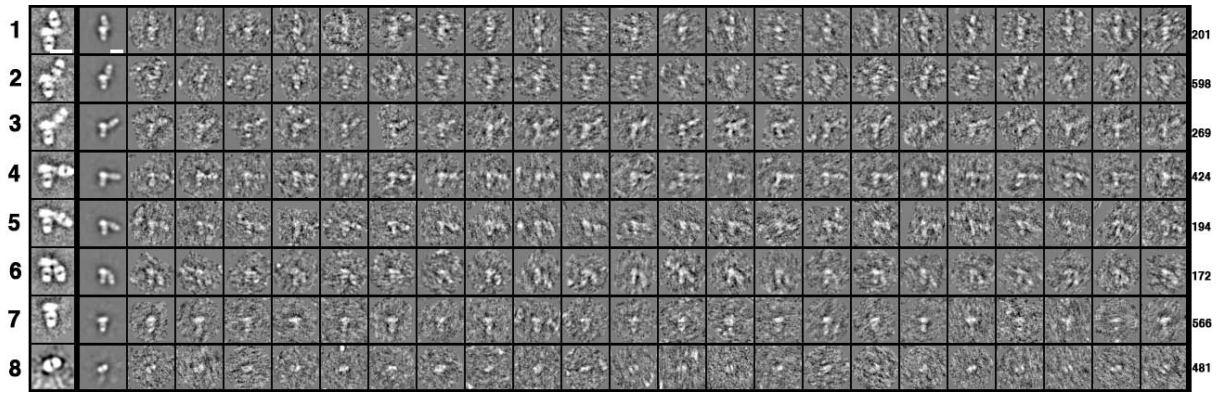

Supplementary Figure 11. Negative-stained reference-free 2D-class averages compared to raw particles. First column entries represent the RCT volume designation shown in Fig. 4b. Second column entries are reference free class averages determined from the untilted micrographs collected at a 150,000x magnification. Classes 7 and 8 are the binary complex of T13 in complex with gp120, and the PG9 Fab, respectively. Third column entries are the reference free class averages determined from the untilted micrographs collected at 62,000x for the RCT image reconstruction. The scale bar in each column is 100Å long. Columns 4-25 are representative raw particles for each class average at the 62,000x magnification. The particles are extracted from CTF corrected images. The final column depicts the total number of particles in each class. A total of 11,997 particles were extracted from the untilted micrographs collected at a 62,000x magnification.

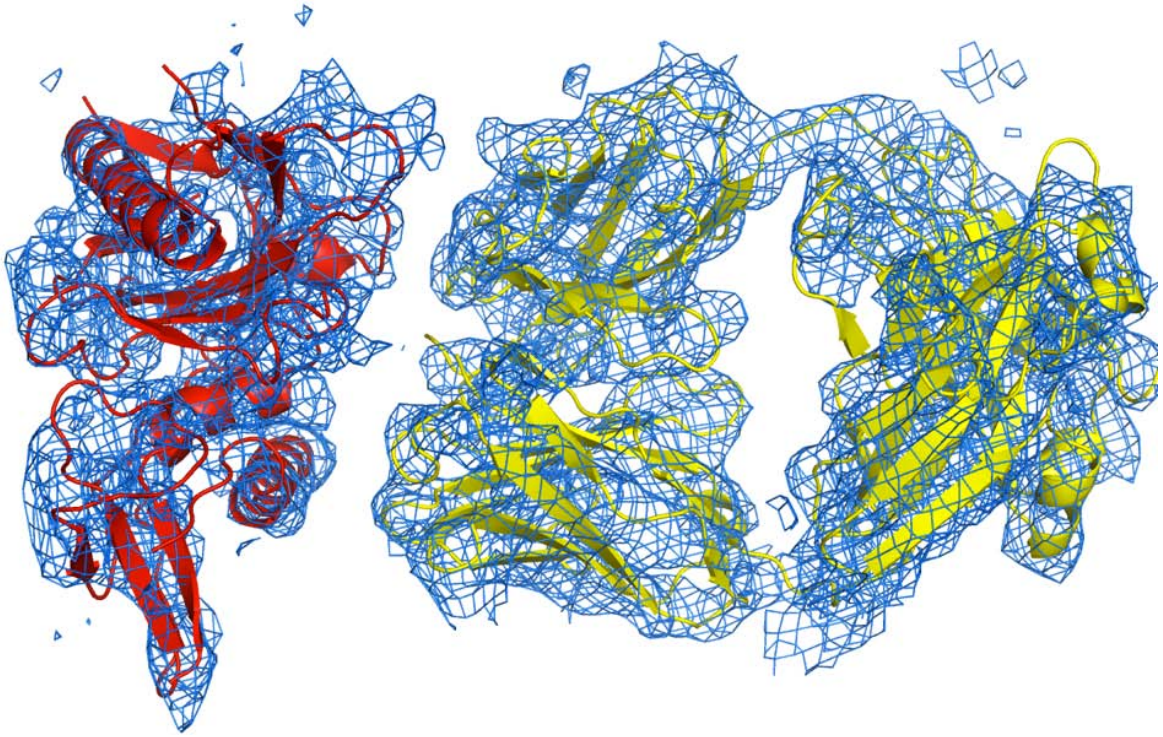

Supplementary Figure 12. 6Å crystal structure of JR-FL gp120 core bound to T13 Fab.
Ribbon representation of JR-FL gp120 core (red) in complex with T13 Fab (yellow) at 6Å with $2F_o$-F_c electron density shown in blue mesh. JR-FL gp120 core was expressed in HEK 293S GnTI$^{-/-}$ cells using a codon-optimized synthetic gene incorporating an Ig kappa signal peptide inserted into the vector phCMV (Genlantis). Cells were transfected with PEIMAX (PolySciences) and allowed to secrete Env for 72 hours. Cell supernatant was concentrated and filtered and loaded on to *Galanthus nivalis* lectin agarose beads (Vector labs) and eluted with 1.0 M methyl-α-d-mannopyranoside. The eluted gp120 was further purified by SEC using Superdex 200 16/60 (GE Healthcare). T13 Fab was expressed by periplasmic secretion of both the light and heavy chains using pET-Duet. Cells were induced with IPTG and allowed to express Fab overnight at 16˚C. Cells were then harvested by centrifugation, protease inhibitor cocktail set V (CalBiochem) was added, and passaged three times through a cell disruptor. Clarified cell lysate was loaded on a 5 mL HiTrap Protein G column and Fab was eluted using 1 M glycine pH 2.8. Affinity-purified Fab was then purified further by Mono S cation exchange. A complex of JR-FL gp120 core and T13 Fab was concentrated to 16 mg/ml and crystallized by sitting drop vapor diffusion in 20% PEG 3350, 0.2 M lithium chloride, 12.5 mM Tris, pH 8.0. Crystals were cryoprotected by addition of 30% glycerol to the mother liquor, and a data set to 6.0 Å was collected. Molecular replacement was carried out with PHASER. A shell script was used to cycle through 176 different Fab models using an in-house database of structurally aligned Fab coordinates derived from the PDB. A solution using F105-bound gp120 (PDB ID: 3HI1), truncated V1/V2 stem and β20-21 loop, and the 176 Fab database placed gp120 and two different Fabs, which yielded the same solution. Env residues 91-116, 210-297, 330-395, 412-491 were used in the structure solution and the Fab from PDB ID 1HZH.
-gp120 solution: rotation (euler) α, β, γ 147.44, -100.52, 2.34; translation vector (Å) 44.20, 62.84, -43.19
-Fab solution: rotation (euler) α, β, γ 62.81, -60.86, 43.98; translation vector (Å) 258.09, 139.37, -93.15
Rigid body refinement was undertaken with PHENIX, and the structure was refined to an R_{cryst} of 0.31 (R_{free} of 0.46). No coordinate refinement was performed.

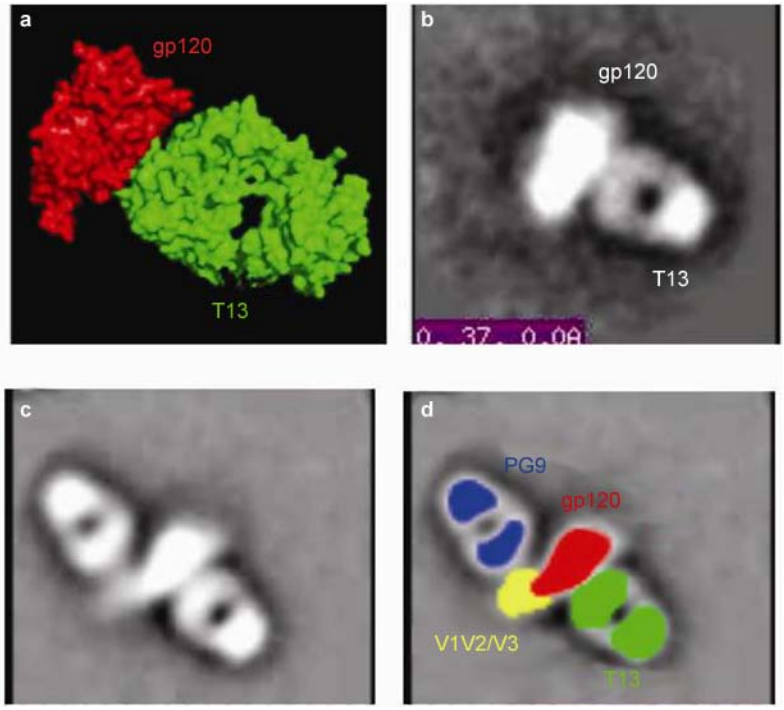

Supplementary Figure 13. Negative stain of gp120-T13 and gp120-T13-PG9 complex.
a, Crystal structure of gp120-T13 complex at 6Å. **b**, 2D class average of the same complex by EM. This view corresponds to view 7 in Supplementary Fig. 11. **c,** 2D class average of ternary complex of gp120-T13-PG9. **d,** Same as **b** but colored by component. This view corresponds to view 1 in Supplementary Fig. 11. Thus, the binary crystal and EM structures unambiguously define the location of T13 on one side of the strong rod-shaped gp120 density. These fits all orient the V1/V2/V3 loops into the additional plume of density adjacent to the other strong density for an Fab, which then is PG9. Additional evidence for this arrangement is provided by an EM titration experiment required to get higher populations of the ternary complex. Briefly, it was necessary to add excess PG9 to the stoichiometric, purified gp120-T13-PG9 complex after diluting the sample in preparation for deposition on the EM grid. Failure to do so resulted in a proportionally higher population of view 7 (Supplementary Fig. 11), which represents the gp120-T13 complex as discussed above.

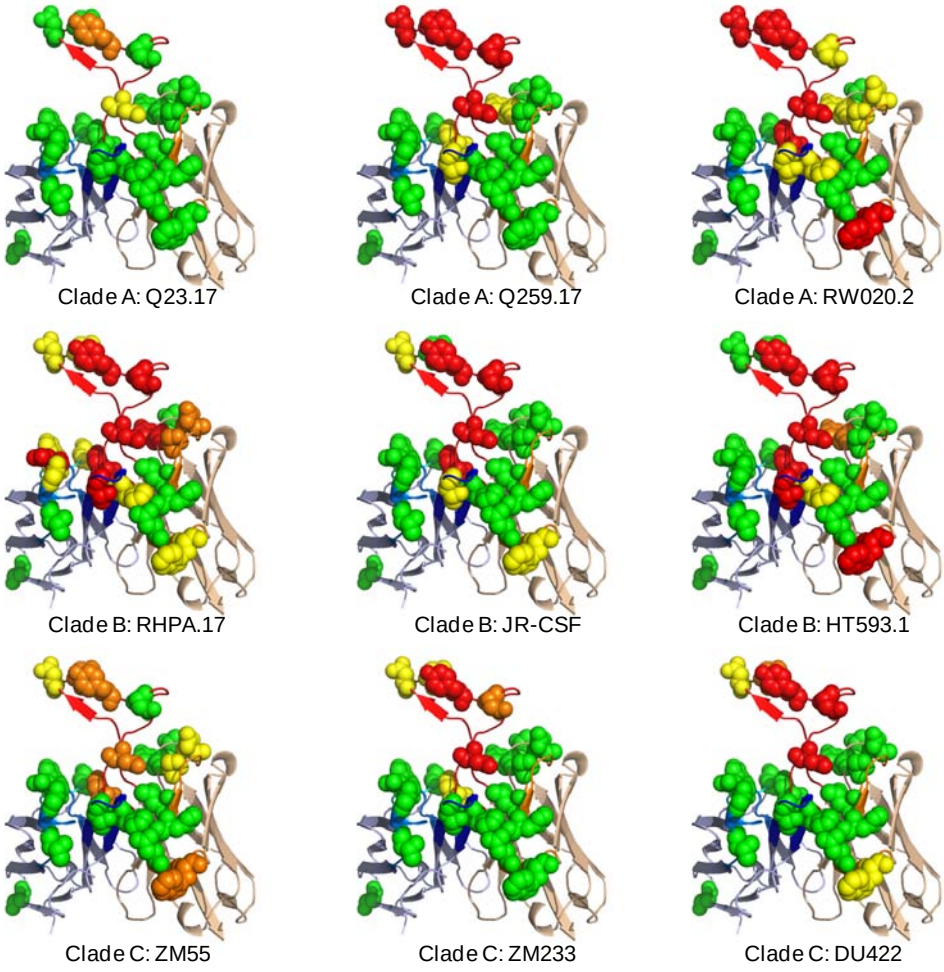

Supplementary Figure 14. Functional definition of PG16 paratope by "arginine-scanning" mutagenesis. 22 individual arginine mutants were assessed for neutralization on nine different strains of HIV-1. Residues mutated to arginine are displayed as spheres on a ribbon diagram of the unbound PG16 structure (Pancera et al., J. Virol., 2010), and colored according to the fold-increase in IC_{50} for the mutant relative to wild-type.

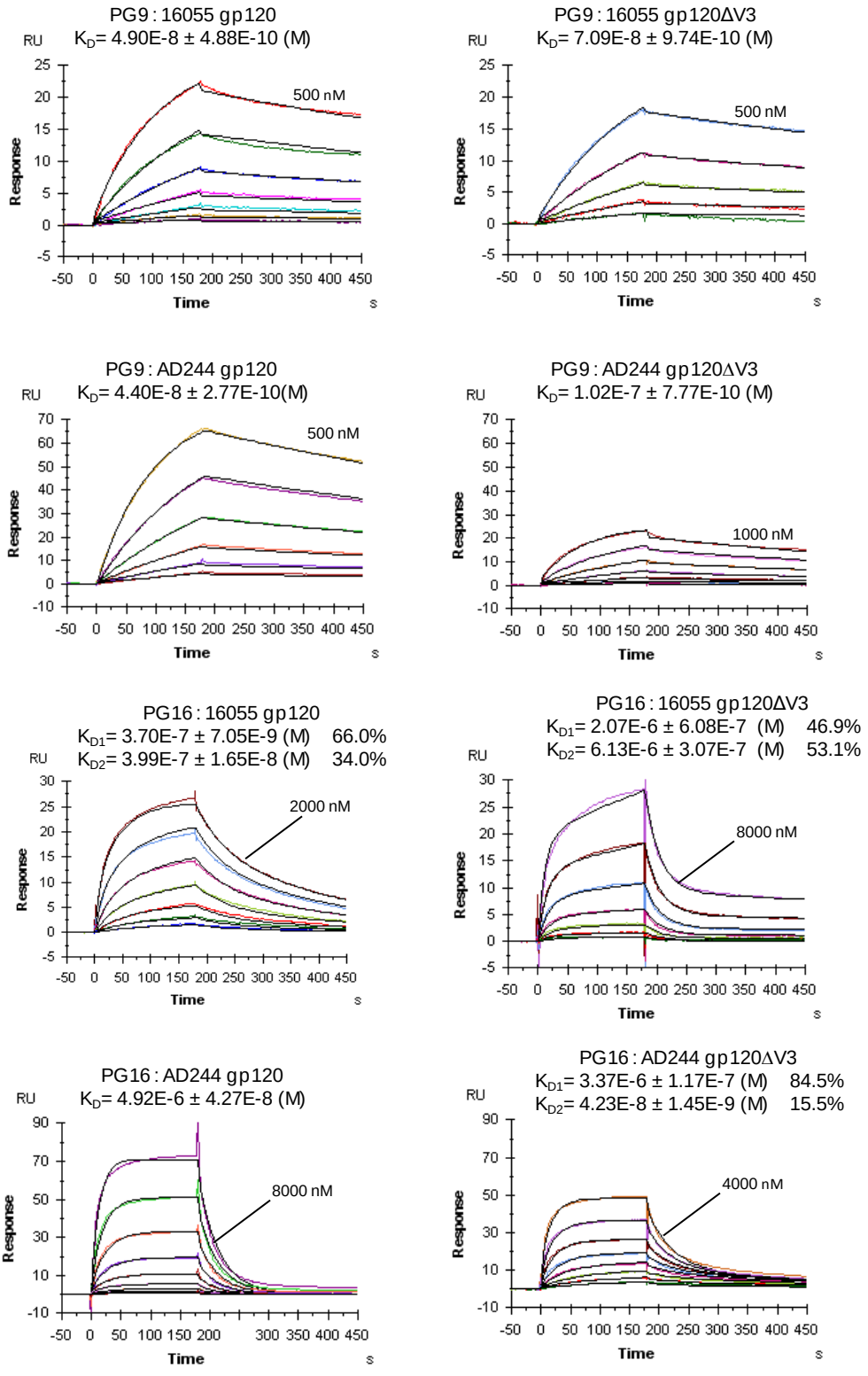

Supplementary Figure 15. PG9 and PG16 binding to gp120 in the presence and absence of the V3 loop. Full-length gp120 monomers (left column) or V3-deleted gp120 monomers (right column) were tested for binding to PG9 (top) and PG16 (bottom). Surface-plasmon resonance sensorgrams with their respective fitted curves (black) are shown, with the highest concentration of each 2-fold dilution series labeled. The equilibrium dissociation constant (K_D) is shown above the sensorgrams. In curves fitted with a heterogenous model, separate K_Ds are listed, along with contributing percentages for each component. Data were processed as described in Methods.

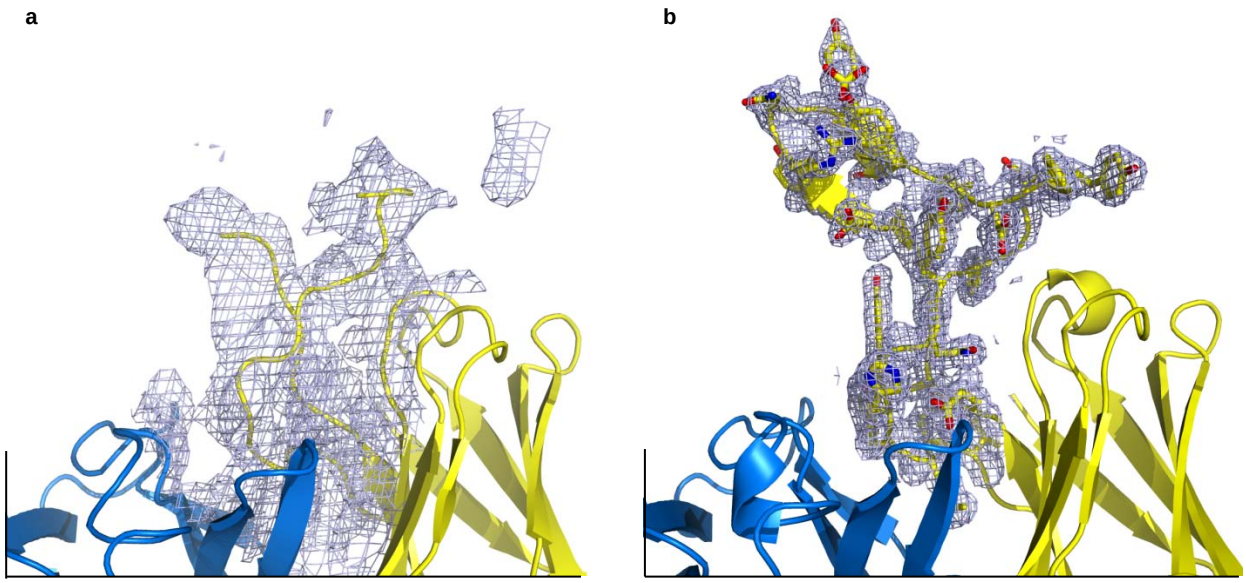

Supplementary Figure 16. PG9 CDR H3 electron density in unbound and V1V2-bound structures. To determine the degree that unbound structures resembled complexed ones, we determined the structure of unbound PG9. PG9 crystals diffracted to 3.3 Å with 4 molecules in the asymmetric unit. In three of the four molecules that comprise the asymmetric unit, the CDR H3 appeared to be completely disordered, with weak density observed for only one molecule, consistent with the unbound PG9 CDR H3 being a highly mobile subdomain; in contrast, other regions of the unbound PG9-variable domains closely resembled the bound structures. We previously determined the unbound structure of PG16, which also displayed a flexible or more mobile CDR H3. Superposition of the unbound PG16 structure with that of PG9 in the PG9-V1V2 complex indicated that somatic differences focused primarily at the region N-terminal to the V1V2-interactive strand of the CDR H3 and to residues involved in glycan recognition. Overall, unbound PG9 and PG16 structures were compatible with an induced fit mechanism of recognition, where CDR H3 mobility enhances the ability of PG9 and PG16 to penetrate the flexible glycan shield that covers V1V2. **a,** Ribbon representation of the unbound PG9 Fab, zoomed in on the CDR H3. Heavy chain is yellow, and light chain is blue. $2F_o$-F_c electron density within 6 Å of the CDR H3 and contoured at 0.7 σ is shown as a light blue mesh **b,** Ribbon representation of the 1FD6-ZM109-bound PG9 Fab, zoomed in on the CDR H3. $2F_o$-F_c electron density within 1.5 Å of the CDR H3 and contoured at 1.0 σ is shown as a light blue mesh.

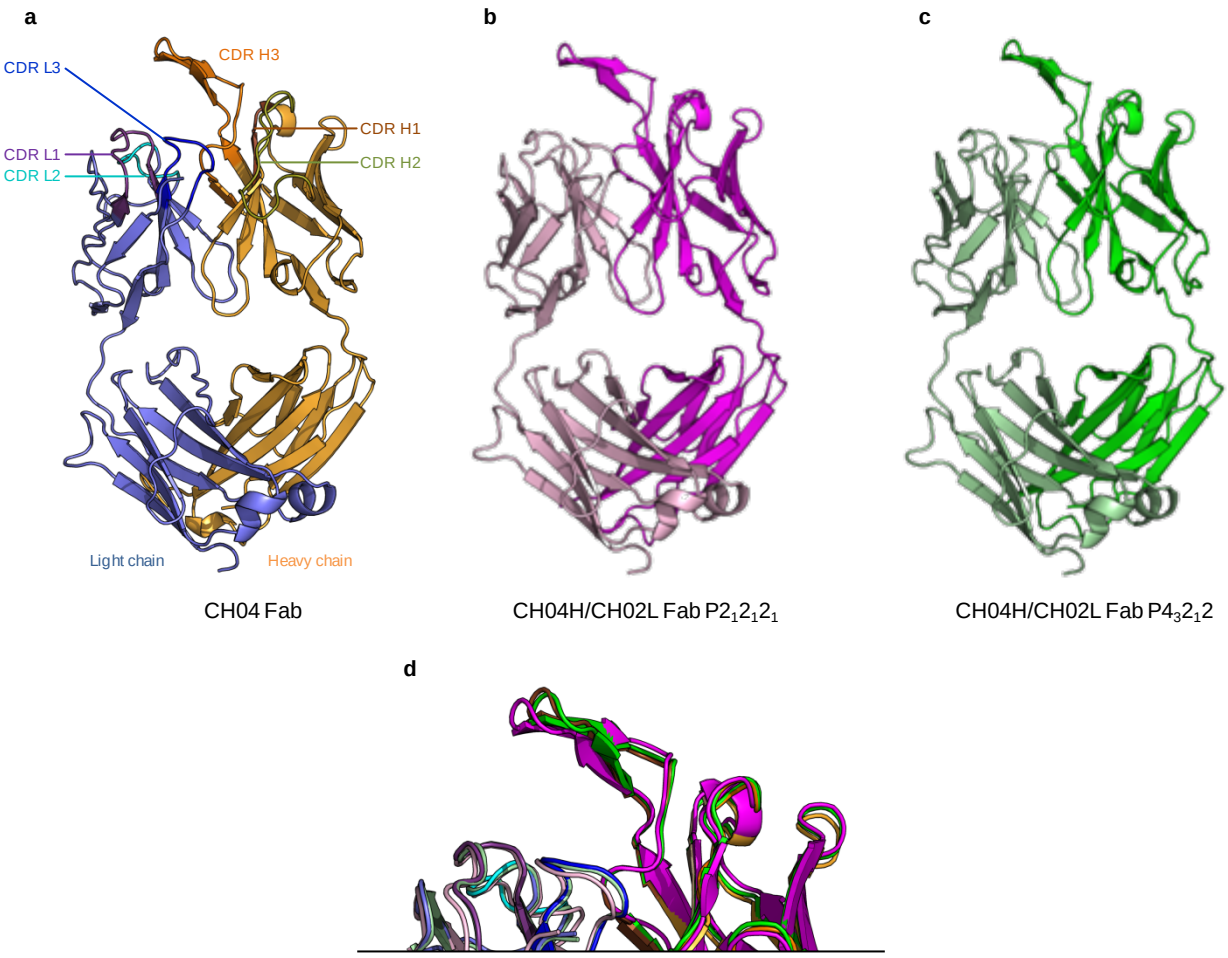

e

Structure	Space group	Common CDR H3 lattice contacts (Heavy Chain:Light Chain)					
		N110:OG203	O110:N203	O110:O201	N112:O201	O112:N113	O107:N155
CH04	$P2_12_12_1$	✓	✓	✓	✓	✓	×
CH04H/CH02L	$P2_12_12_1$	✓	✓	✓	✓	✓	×
CH04H/CH02L	$P4_32_12$	✓	✓	✓	✓	✓	✓

Supplementary Figure 17. Unbound structures of CH04 Fab and of chimeric CH04H/CH02L Fab. Antibodies CH01-CH04 form a clonal lineage, identified from a clade A-infected donor (CHAVI-0219), with heavy chain-derived from the VH3 family, the same as PG9/PG16 (Bonsignori et al., J. Virol., 2011). Neutralization characteristics of CH01-04 closely resemble those of PG9 and PG16, with a highly similar, alanine-mutagenesis-defined, target epitope. Fabs of CH01-CH03 formed small needles, which were not suitable for structural analysis (Supplementary Table 20). CH04 formed orthorhombic crystals that diffracted to 1.9 Å, with two molecules in the asymmetric unit, and structure determination and refinement led to an R_{cryst} of 19.6% (R_{free} = 23.8%) (Supplementary Table 19). Chimeric Fabs of CH04H/CH02L formed orthorhombic and tetragonal crystals that diffracted to 2.9 Å. **a.** Unbound structure of Fab CH04. Ribbon diagram displays heavy (orange) and light (blue) chains, with CDRs shaded as indicated. **b.** Unbound structure of orthorhombic Fab CH04H/CH02L. Ribbon diagram displays heavy (magenta) and light (light pink) chains. **c**. Unbound structure of tetragonal Fab CH04H/CH02L. Ribbon diagram displays heavy (green) and light (light green) chains. **d.** Superposition of the CDR H3s with color described in **a**, **b** and **c**. **e.** CDR H3 lattice contacts.

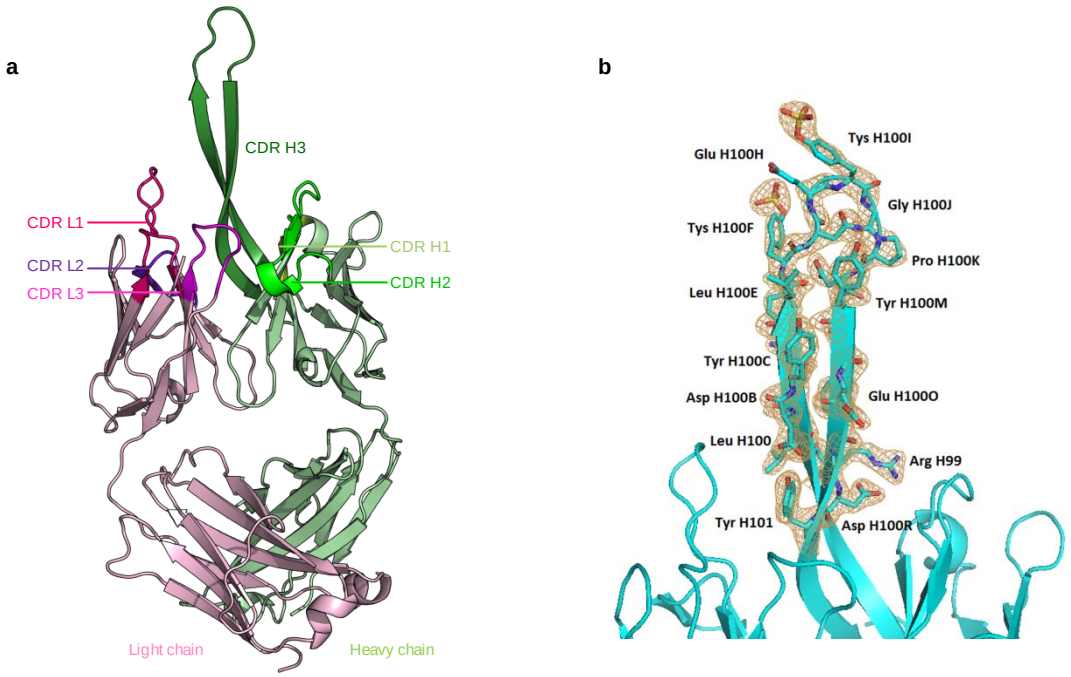

Supplementary Figure 18. Unbound structure of PGT145 Fab.
Antibodies PGT141-145 form a clonal lineage, identified from a clade A- or D-infected donor (IAVI protocol G-84), with heavy chain-derived from the VH1 family (Walker et al., Nature, 2011). Neutralization characteristics of PGT141-145 closely resemble those of PG9 and PG16, although PGT145, the most effective member of this lineage, appeared to have greater tolerance for the type of glycan. Crystals of PGT145 diffracted to 2.3 Å, with 1 molecule in the asymmetric unit, and structure determination and refinement lead to an R_{cryst} of 19.1% (R_{free} = 22.6%) (Supplementary Table 19). **a.** Ribbon diagram displays heavy (green) and light (pink) chains, with CDRs shaded as indicated. **b**. PGT145 CDR H3 details with $2F_o$-F_c electron contoured at 1 σ shown in brown.

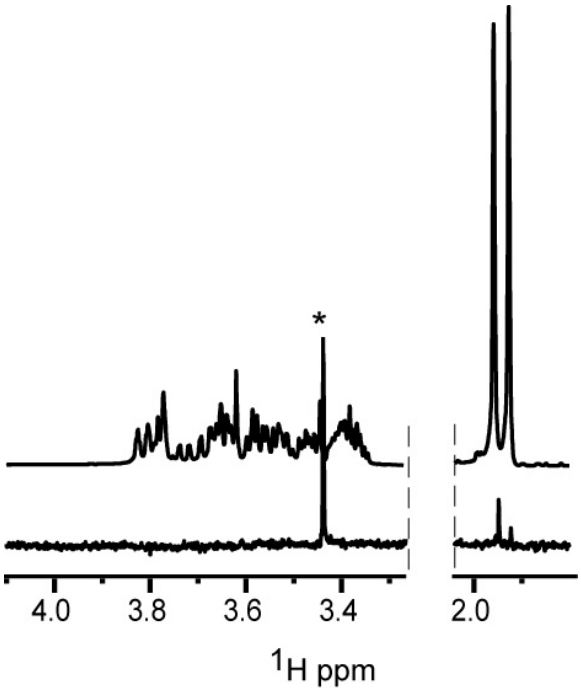

Supplementary Figure 19. Binding of GlcNAc2 to PG9 by NMR.
STD (lower) and reference (upper) NMR spectra of 1.5 mM GlcNAc2 in the presence of 15 μM Fab PG9. (*) Buffer impurity exhibiting nonspecific binding to PG9.

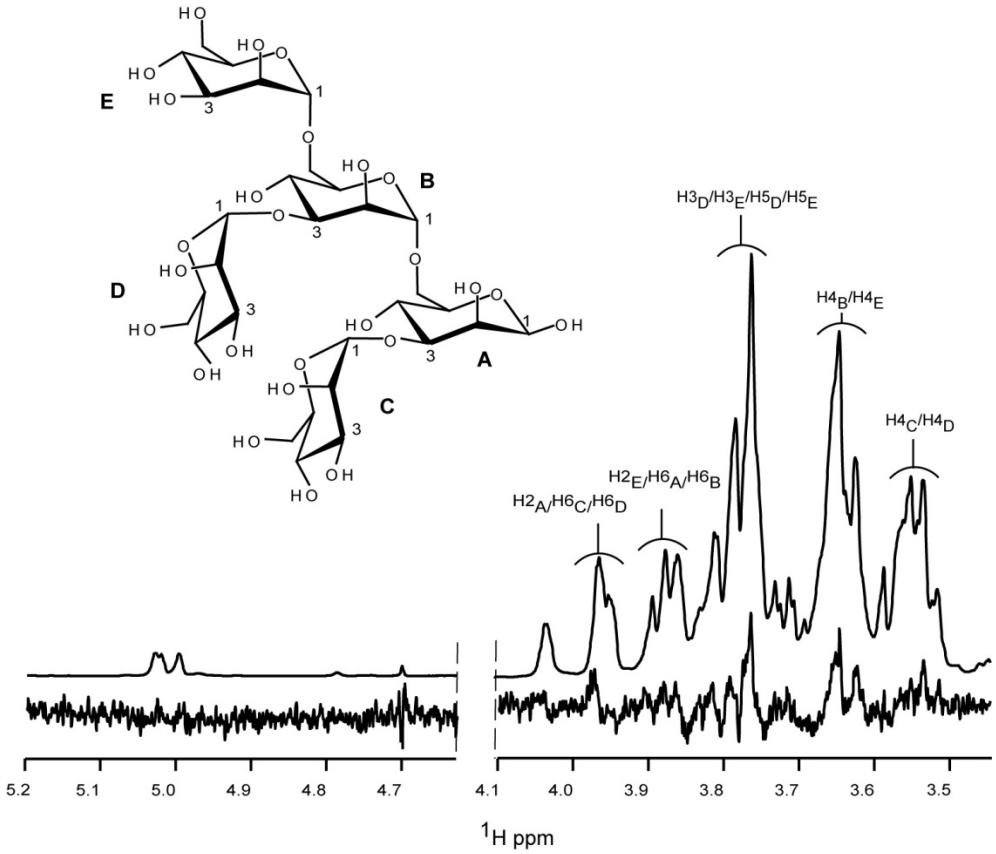

Supplementary Figure 20. Binding of mannopentaose to PG9 by NMR.
STD (lower) and reference (upper) NMR spectra of 1.5 mM mannopentaose (structure shown above) in the presence of 15 μM Fab PG9. Protons that exhibit STD enhancements are labeled.